Dynamics of a superfluid helium nanodroplet doped with a single potassium atom

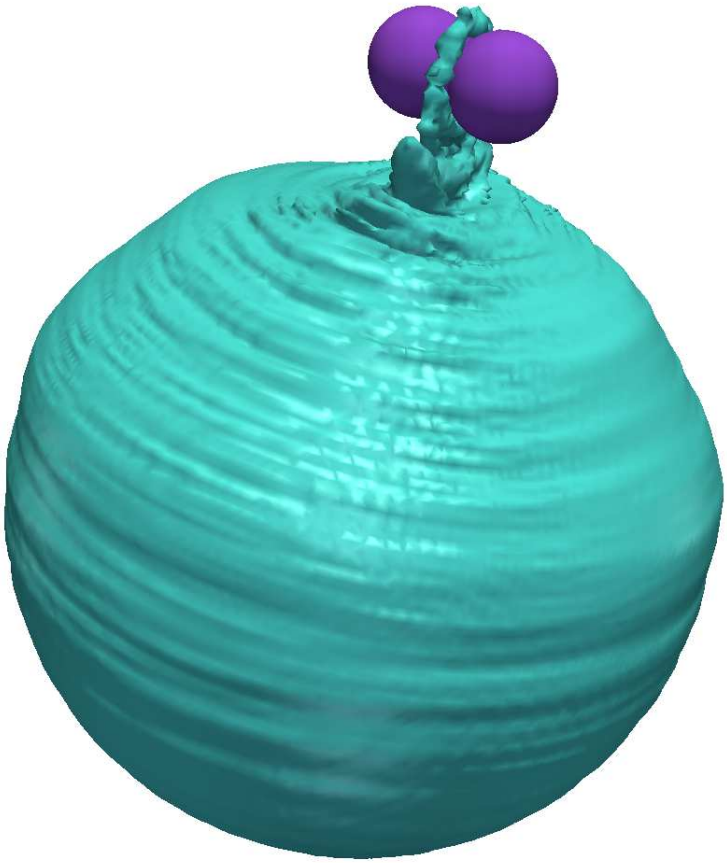

Maxime Martinez [⊛]

M2 *Physique Fondamentale*, Université Toulouse III Paul Sabatier

Under the supervision of N. Halberstadt [⊛] *and F.* Coppens [⊛]
In tight collaboration with M. Barranco [⊛⊙] *and M.* Pí [⊙]

[⊛] *Laboratoire des Collisions, Agrégats, Réactivité, IRSAMC, UMR 5589, CNRS et Université Toulouse III Paul Sabatier, 118 route de Narbonne, Toulouse Cedex, France*
[⊙] *Departament FQA, Facultat de Física, and IN2UB, Universitat de Barcelona, Diagonal 645, 08028 Barcelona, Spain*

UNIVERSITÉ TOULOUSE III PAUL SABATIER — Université Fédérale Toulouse Midi-Pyrénées

IRSAMC — LCAR - LCPQ - LPCNO - LPT

Contents

Introduction

In this work we describe the dynamics following photoexcitation of a potassium atom on a 4-helium nanodroplet. 4-Helium nanodroplets are ultra cold clusters (0.37 K) of typically 10^3 up to 10^6 helium atoms. This fascinating environment has been the focus of a whole community's interest for more than 30 years. The reader should refer to the two nice review papers by Toennies et al. [1, 2] and the one by Barranco et al. [3] which give a more detailed presentation of this topic.

At first, 4-helium droplets were studied for their own, intrinsic interest. Indeed, 4-helium is known to be superfluid at low temperature. Nevertheless superfluidity is usually defined as a macroscopic behavior. Hence these droplets are ideal candidates to address the definition of super-fluidity in a finite range system and its link to Bose-Einstein condensation. Several experimental evidences have been found to characterize their superfluidity. The most intuitive one is the free rotation of molecules embedded in droplets: spectroscopy experiments exhibited resolved rotational spectra [4], which is not possible within a classical fluid. However, the true evidence for superfluidity came from the excitation spectra of super-fluids predicted by Landau from hydrodynamic equations. The existence of a roton gap and a critical velocity have been demonstrated in droplets [5]. The quantum nature of droplets makes it possible to study other fundamental phenomena, such as quantized vortices [6, 7].

Beyond their intrinsic fundamental interest, these have also become a true nano-laboratory thanks to their unique properties. We already talked about rotational spectroscopy study (most dopants are heliophilic and reside in the middle of the droplet). Droplets are also used to investigate alignment of molecules in an electromagnetic field within the droplet [8, 9], the formationation of metal nano-clusters and nanowires [10], *etc.* [1, 2].

We are interested in the doping of a helium droplet by a single potassium atom. Alkali atoms have been demonstrated to reside in a dimple at the surface of the droplet [11], *id est* they are one of the few species for which the potential interaction with He is weaker than the He-He interaction, which makes them heliophobic.

Most of alkali dopants have been intensively investigated by spectroscopy studies[12–18] which can probe accessible states for the attached impurity. Upon excitation to non highly-repulsive states, the formation of exciplexes (stable Alk*-He$_n$ with $n \sim 1-6$) or the desorption of free atom have been observed [13, 15, 19–21]. These phenomena have been addressed from both the theoretical and the computational point of view within a ^{4}He-time-dependent density functional theory (^{4}He-TDDFT) framework and a Diatomics In Molecules (DIM) model [16, 18, 22, 23]. This method has proved to be the best compromise between accuracy and ability to describe droplets of realistic sizes.

We present in the following a ^{4}He-TDDFT simulation of the dynamics following of ($4p \leftarrow 4s$) and ($5s \leftarrow 4s$) excitation of potassium from the equilibrium configuration of a K-He$_N$ droplet with $N = 1000$. The choice of potassium is motivated by a discrepancy in time resolved experimental studies [19–21]. Furthermore, potassium is intermediate between the heavier alkalis (Rb, Cs) which could successfully be described using classical dynamics, and the lighter ones (Li, Na), which clearly require a quantum mechanical description. In this work we test both treatment for the static, equilibrium properties and for the ($5s \leftarrow 4s$) excitation.

1. Theory

1.1 The density functional theory (DFT) applied to a bosonic system

1.1.1 Basic ideas on DFT

Fundamental theorem

Let us start by defining our system: we will be considering a droplet of N helium atoms described by the many-body wavefunction $\Phi(\mathbf{r}_1, \ldots, \mathbf{r}_N)$. We introduce the density $\rho(\mathbf{r})$ as

$$\rho(\mathbf{r}) = \langle \Phi | \, \hat{\rho} \, | \Phi \rangle = \langle \Phi(\mathbf{r}_1, \ldots, \mathbf{r}_N) | \sum_{i=1}^{i=N} \delta(\mathbf{r} - \mathbf{r}_i) \, | \Phi(\mathbf{r}_1, \ldots, \mathbf{r}_N) \rangle \tag{1.1}$$

The density functional theory mostly consists in finding ground state properties. It relies on the HOHENBERG-KOHN theorem [24] which states that the lowest energy configuration is fully determined by the density.

> **Theorem.** The external potential (and hence the total energy), is a unique functional of the density. The functional that delivers the ground state energy of the system, gives the lowest energy if and only if the input density is the true ground state density.

One commonly uses the so-called KOHN-SHAM approach, which consists in writing the total energy of the system in the following way

$$E[\rho] = \int \mathrm{d}\mathbf{r} \, \{\mathcal{T}[\rho] + \mathcal{E}_c[\rho]\} \tag{1.2}$$

In this expression $\mathcal{T}$ represents the kinetic energy of a non-interacting set of particles, and $\mathcal{E}_c$ the interaction in a very general way. The crucial point in the DFT is the explicit form for the functional $\mathcal{E}_c[\rho]$. There is no procedure to get it. Hence one has to resort to physical intuition to choose a form and to fit its parameter values.

Bosonic formulation

Helium 4 is a boson, and the temperature of the droplets has been determined to be of 0.37 K in usual experimental conditions. We thus assume that the system is fully condensed in a given state whose associated wave function is denoted as φ_0

$$|\Phi(\mathbf{r}_1, \ldots, \mathbf{r}_N)\rangle = \prod_{i=1}^{i=N} \varphi_0(\mathbf{r}_i) \quad \text{hence} \quad \rho(\mathbf{r}) = N|\varphi_0(\mathbf{r})|^2 \tag{1.3}$$

Also, we introduce an *order parameter* (also called *effective wave function*) which actually almost corresponds to the single-body wave-function and will lead to simpler equations

$$\Psi(\mathbf{r}) \equiv \sqrt{\rho(\mathbf{r})} \, \mathrm{e}^{i\mathcal{S}(\mathbf{r})} \Rightarrow \Psi(\mathbf{r}) = \sqrt{N} \, \varphi_0(\mathbf{r}) \tag{1.4}$$

1.1.2 Analytic expressions for the functional

Kinetic energy

The purpose of the KOHM-SHAM formulation is to make the expression of kinetic energy simple. Using (1.3) and denoting by m_{He} the helium atom mass, we have

$$\mathcal{T}[\rho] = -\frac{\hbar^2}{2m_{\mathrm{He}}} \langle \Phi | \nabla^2_{\mathbf{r}_i} | \Phi \rangle = -N \frac{\hbar^2}{2m_{\mathrm{He}}} \langle \varphi_0 | \nabla^2 | \varphi_0 \rangle = \frac{\hbar^2}{2m_{\mathrm{He}}} \int \mathrm{d}\mathbf{r} \, (\nabla \Psi)^2 \tag{1.5}$$

$\mathcal{E}_c$ Orsay-Trento Complete (OTC) functional and its simplified version (OT)

The choice of a functional for $\mathcal{E}_c$ is actually the decisive point in a DFT calculation. We do not discuss here how to find such an analytic expression, the interested reader may refer to [3]. We simply present the most accurate one, which has been successfully used in a number of studies [3, 7] (the values for the parameters can be found in the annex d)

$$\begin{aligned}\mathcal{E}_c[\rho] = \frac{1}{2} \int \mathrm{d}\mathbf{r}' \, \rho(\mathbf{r}) V_{\mathrm{LJ}}(|\mathbf{r}-\mathbf{r}'|)\rho(\mathbf{r}') + \frac{c_2}{2} \rho(\mathbf{r})[\bar{\rho}(\mathbf{r})]^2 + \frac{c_3}{3} \rho(\mathbf{r})[\bar{\rho}(\mathbf{r})]^3 \\ -\frac{\hbar^2}{4m} \alpha_s \int \mathrm{d}\mathbf{r}' \, \tilde{\omega}(|\mathbf{r}-\mathbf{r}'|) \left(1 - \frac{\tilde{\rho}(\mathbf{r})}{\rho_0}\right) \boldsymbol{\nabla}_{\mathbf{r}}[\rho(\mathbf{r})] \cdot \boldsymbol{\nabla}_{\mathbf{r}'}[\rho(\mathbf{r}')] \left(1 - \frac{\tilde{\rho}(\mathbf{r}')}{\rho_0}\right) \\ -\frac{m}{4} \int \mathrm{d}\mathbf{r}' \, V_{\mathrm{J}}(|\mathbf{r}-\mathbf{r}'|)\rho(\mathbf{r})\rho(\mathbf{r}')[\mathbf{v}(\mathbf{r}) - \mathbf{v}(\mathbf{r}')]^2\end{aligned} \tag{1.6}$$

In (1.6) we have introduced two averaged densities

$$\bar{\rho}(\mathbf{r}) = \int \mathrm{d}r' \, \rho(\mathbf{r}') \, \bar{\omega}(|\mathbf{r}-\mathbf{r}'|) \quad \text{with} \quad \bar{\omega}(\mathbf{r}) = \begin{cases} \frac{3}{4\pi h^3} & r < h \\ 0 & \text{otherwise} \end{cases} \tag{1.7}$$

$$\tilde{\rho}(\mathbf{r}) = \int \mathrm{d}r' \, \rho(\mathbf{r}') \, \tilde{\omega}(|\mathbf{r}-\mathbf{r}'|) \quad \text{with} \quad \tilde{\omega}(\mathbf{r}) = \frac{1}{(\sqrt{\pi} l)^3} \, \mathrm{e}^{-(r/l)^2} \tag{1.8}$$

a truncated LENNARD-JONES potential

$$V_{\mathrm{LJ}}(\mathbf{r}) = \begin{cases} 4\varepsilon_{\mathrm{LJ}} \left(\left(\frac{\sigma}{r}\right)^{12} - \left(\frac{\sigma}{r}\right)^{6} \right) & r > h \\ 0 & \text{otherwise} \end{cases} \tag{1.9}$$

and an effective current-current interaction that mimics the back flow contribution, fitted to reproduce the maxon-roton dispersion curve in liquid ^{4}He, with the velocity $\mathbf{v}(\mathbf{r})$ defined as a function of to the current density $\mathbf{j}(\mathbf{r})$.

$$V_{\mathrm{J}}(r) = (\gamma_{11} + \gamma_{12} r^2) \, \mathrm{e}^{-\alpha_1 r^2} + (\gamma_{21} + \gamma_{22} \, r^2) \, \mathrm{e}^{-\alpha_2 r^2} \tag{1.10}$$

$$\mathbf{v}(\mathbf{r}) = \frac{\mathbf{j}(\mathbf{r})}{\rho(\mathbf{r})} \quad \text{with} \quad \mathbf{j}(\mathbf{r}) = -\frac{i\hbar}{2m_{\mathrm{He}}} [\Psi^*(\mathbf{r}) \boldsymbol{\nabla} \Psi(\mathbf{r}) - \Psi(\mathbf{r}) \boldsymbol{\nabla} \Psi^*(\mathbf{r})] \tag{1.11}$$

Note that this last term is important to accurately reproduce the dispersion curve in liquid ^{4}He, but not in dopant dynamics. Hence since it is computationally more expensive, it is usually neglected in our simulations. This constitutes the OT version.

$\mathcal{E}_c$ solid functional

The previous expression is known to be very accurate. However, numerical instabilities appear when the density reaches values close to that of the solid, which is the case around very attractive dopants. In this case we have used a modification of the OT functional which has been developed to describe bulk liquid helium and the liquid-solid transition [25]: the so-called solid functional

$$\mathcal{E}_c[\rho] = \frac{1}{2}\int \mathrm{d}\mathbf{r}'\,\rho(\mathbf{r})V_{\mathrm{LJ}}(|\mathbf{r}-\mathbf{r}'|)\rho(\mathbf{r}') + \frac{c_2}{2}\,\rho(\mathbf{r})\bar{\rho}(\mathbf{r})^2 + \frac{c_3}{3}\,\rho(\mathbf{r})\bar{\rho}(\mathbf{r})^3 + C\rho(\mathbf{r})\{1+\tanh(\beta[\rho(\mathbf{r})-\rho_m])\} \quad (1.12)$$

1.2 DIM approach: a mean-field description of the interaction between K and $^4\mathrm{He}_N$

1.2.1 General principle

So far, we have discussed how to deal with a pure helium droplet. In order to describe the full KHe_N system, we now turn to the interaction part. The following discussion will be presented in a quite general way.

The total interaction of K with the droplet is approximated by a sum of pair-wise diatomic interactions. This is justified since He is a rare gas atom and the K-He interaction is weak. The validity of this approximation (and of the pair-wise potentials used) is tested by calculating the absorption spectra, see section 2.2.1. This is the so-called *Diatomic In Molecules* (DIM) model [26]. We first describe the case of a single KHe diatomic and then move on to the KHe_N interaction.

1.2.2 The diatomic case: K-He

The standard Born-Oppenheimer approximation states that the fast electronic motion of electrons can be decoupled from the slow nuclei one. From a mathematical point of view, one has to solve the Schrödinger equation for the motion of the electrons for fixed nuclei positions treated as parameters (so-called *electronic* Schrödinger *equation).* This results in a set of eigenvalues $V_\beta(\mathbf{r})$ which constitute the interaction potentials between nuclei in the different possible electronic states labeled with $\{\beta\}$ as quantum numbers.

Potassium is an alkali, hence it can be described as a one active electron system. We introduce different operators that will be useful to characterize its electronic states: orbital ($\mathbf{L}$), spin ($\mathbf{S}$) and total ($\mathbf{J}=\mathbf{L}+\mathbf{S}$) angular momentum, that actually refers to the single electron. In particular, we will be using three different quantum numbers (others than n and l): Λ (L_z), Ω (J_z) and J ($\mathbf{J}^2$), where z is the internuclear axis.

Because of cylindrical symmetry, L_z commutes with the electronic Hamiltonian (in the absence of spin-orbit coupling) and Λ is then a good quantum number. Even though the atomic quantum numbers n and l are mixed in principle, the interaction with helium is rather weak and we can consider effective (nl) orbitals to describe the subspace of electronic states going asymptotically to He + K(nl). No analytical expression is obtained for the radial components as it is not needed, but the angular part is assumed to be the usual spherical harmonics orbitals. Moreover, for computing facilities, we will be working in the basis set of "real spherical harmonics" (combinations of $Y_{l,\pm\Lambda}$, which implies to

change basis when including spin-orbit coupling).

Our study involves three different nl-states: $(4s)$, $(4p)$ and $(5s)$. Let us first neglect spin-orbit coupling. While the s-state interaction is simple, the p-state one splits into two different states with Λ as a good quantum number.

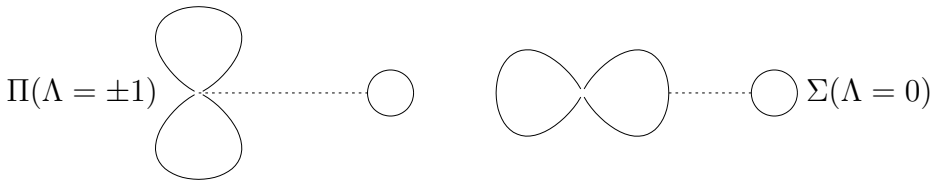

Figure 1.1 – Illustration and labeling of energy level splitting in K(np) state interaction with He

We assume that spin-orbit coupling is the same that in free atom ($A_{\rm LS}$ for free K from [27])

$$H^{nl/\rm SO} = A_{\rm LS}\,\mathbf{L}\cdot\mathbf{S} \tag{1.13}$$

We know that s-states are not affected (they are just doubly degenerated since $S = 1/2$), but p-states get an additional energy splitting, with good quantum number Ω (because $J_z = L_z + S_z$ obviously commutes with the spin-orbit Hamiltonian but also with the electrostatic interaction one since L_z (and S_z) do). It is therefore important to note that when electrostatic interaction is large *id est* at short distances then Λ is almost a good quantum number and in the opposite way at large distances it is J.

In practice we start from PASCALE [28] $V_\Sigma^{4p}(\mathbf{r})$, $V_\Pi^{4p}(\mathbf{r})$, $V^{5s}(\mathbf{r})$ and PATIL [29] $V^{4s}(\mathbf{r})$ pair potentials that do not include spin-orbit coupling. The electrostatic interaction is expressed as

- for the ground state: $(4s)$

$$H^{4s}(\mathbf{r}) = V^{4s}(\mathbf{r})\,|4s\rangle\,\langle 4s| \tag{1.14}$$

- for the first excited p-state: $(4p)$

$$\begin{aligned} H^{4p}(\mathbf{r}) &= V_\Pi^{4p}(\mathbf{r})\{|4p_x\rangle\,\langle 4p_x| + |4p_y\rangle\,\langle 4p_y|\} + V_\Sigma^{4p}(\mathbf{r})\,|4p_z\rangle\,\langle 4p_z| \\ &= V_\Pi^{4p}(\mathbf{r})\cdot\mathbb{I}_3 + [V_\Sigma^{4p}(\mathbf{r}) - V_\Pi^{4p}(\mathbf{r})]\,|4p_z\rangle\,\langle 4p_z| \end{aligned} \tag{1.15}$$

- for the first excited s-state: $(5s)$

$$H^{5s}(\mathbf{r}) = V^{5s}(\mathbf{r})\,|5s\rangle\,\langle 5s| \tag{1.16}$$

The total electronic Hamiltonian is then written as the sum of the electrostatic interaction denoted ES and the spin orbit coupling denoted SO

$$H^{nl}_{\rm K-He} = H^{nl/\rm ES}_{\rm K-He} + H^{nl/\rm SO} = H^{nl/\rm ES}_{\rm K-He} + A_{\rm LS}\,\mathbf{L}\cdot\mathbf{S} = H^{nl/\rm ES}_{\rm K-He} + \frac{A_{\rm LS}}{2}(\mathbf{J}^2 - \mathbf{L}^2 - \mathbf{S}^2) \tag{1.17}$$

1.2.3 DIM and mean-field theory

We need to introduce a set of orbitals as a basis for our study. We choose the **uncoupled basis of real orbitals oriented along the pseudo-internuclear axis** (fig. 1.2) denoted $\{|nl_i, \pm\rangle\}$, where nl_i refers to the i-th spatial orbital associated with the (nl) state and $\pm$ refers to the spin state (actually $\pm 1/2$ since $S = 1/2$). For instance in the $nl = 4p$ case, the basis is $\{|4p_x, \pm\rangle, |4p_y, \pm\rangle, |4p_z, \pm\rangle\}$, while for ns states the basis is $\{|ns, \pm\rangle\}$. As we already said: the principle of this approach is to write the total electrostatic Hamiltonian as the sum over all pair contributions

$$H^{nl}_{\mathrm{K-He}_N} = \sum_{m=1}^{m=N} H^{nl/\mathrm{ES}}_{\mathrm{K-He}}(\mathbf{r}_m) + H^{nl/\mathrm{SO}} \equiv H^{nl/\mathrm{ES}}_{\mathrm{K-He}_N} + H^{nl/\mathrm{SO}} \tag{1.18}$$

Here is a tricky point: the m-th pair-interaction Hamiltonian in (1.18) is actually expressed in a set of orbitals defined in the axes attached to the m-th internuclear axis, but we want this one to be expressed in the previously chosen basis, common to all pairs. We then need to express those pair Hamiltonians in the common basis. This is done by applying a rotation $\mathcal{R}_m : \hat{\mathbf{z}}_m \longmapsto \hat{\mathbf{z}} \propto \mathbf{r}_\mathrm{K}$ (which depends on the angular momentum)

$$H^{nl/\mathrm{ES}}_{\mathrm{K-He}_N} = \sum_{m=1}^{m=N} \mathcal{R}_m^{-1} H^{nl/\mathrm{ES}}_{\mathrm{K-He}}(\mathbf{r}_m)\, \mathcal{R}_m \tag{1.19}$$

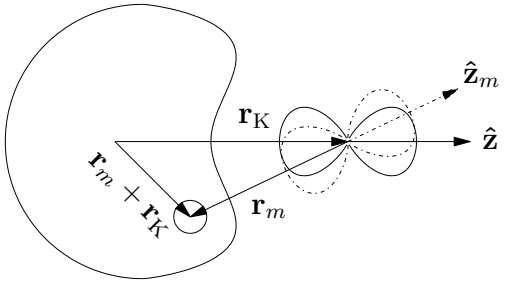

Figure 1.2 – Set of axes involved in our description

We now define $U^{nl}_{ij\alpha\beta}$ which is simply the pair-interaction Hamiltonian expressed in the common basis

$$U^{nl/\mathrm{ES}}_{ij\alpha\beta}(\mathbf{r}_m) = \langle i, \alpha|\, \mathcal{R}_m^{-1} H^{nl/\mathrm{ES}}_{\mathrm{K-He}}(\mathbf{r}_m)\, \mathcal{R}_m\, |j, \beta\rangle \tag{1.20}$$

The matrix elements of the total electrostatic Hamiltonian can then be expressed in the discrete case (helium atoms) or in the continuum case (helium density) as

$$E^{nl/\mathrm{ES}}_{ij\alpha\beta}(\{\mathbf{r}_m\}) = \sum_{m=1}^{m=N} U^{nl/\mathrm{ES}}_{ij\alpha\beta}(\mathbf{r}_m) \tag{1.21}$$

$$E^{nl/\mathrm{ES}}_{ij\alpha\beta}(\mathbf{r}_\mathrm{K}) = \int \mathrm{d}\mathbf{r}\, \rho(\mathbf{r} + \mathbf{r}_\mathrm{K})\ \langle i, \alpha|\, \mathcal{R}^{-1}(\mathbf{r}) H^{nl/\mathrm{ES}}_{\mathrm{K-He}}(\mathbf{r})\, \mathcal{R}(\mathbf{r})\, |j, \beta\rangle \equiv \int \mathrm{d}\mathbf{r}\, \rho(\mathbf{r} + \mathbf{r}_\mathrm{K})\, U^{nl/\mathrm{ES}}_{ij\alpha\beta}(\mathbf{r}) \tag{1.22}$$

Spherically symmetric (ns) state

Let us first consider the two (ns) states: $(4s)$ and $(5s)$. They are particularly easy to treat because the spin-orbit coupling can be omitted since $L = 0$ (see eq. 1.13). We are left with the electrostatic contribution, which is also easy to express because s-states are spherically symmetric, hence invariant

under rotation about they symmetry center

$$\begin{aligned} U^{ns/\mathrm{ES}}_{ij\alpha\beta}(\mathbf{r}_m) &= \langle i,\alpha|\,\mathcal{R}_m^{-1} H^{nl/\mathrm{ES}}_{\mathrm{K-He}}(\mathbf{r}_m)\,\mathcal{R}_m\,|j,\beta\rangle \\ &= V^{ns}(\mathbf{r}_m)\ \langle i,\alpha|\,\mathcal{R}_m^{-1}\,|ns_m\rangle\,\langle ns_m|\ \mathcal{R}_m\,|j,\beta\rangle \\ &= V^{ns}(\mathbf{r}_m)\ \langle i,\alpha|ns_m\rangle\,\langle ns_m|j,\beta\rangle \\ &= V^{ns}(\mathbf{r}_m)\,\delta_{ij}\delta_{\alpha\beta} \end{aligned} \tag{1.23}$$

$$E^{ns/\mathrm{ES}}_{ij\alpha\beta}(\mathbf{r}_\mathrm{K}) = \int \mathrm{d}\mathbf{r}\,\rho(\mathbf{r}+\mathbf{r}_\mathrm{K})\,V^{ns}(\mathbf{r})\,\delta_{ij}\delta_{\alpha\beta} \tag{1.24}$$

The matrix elements are clearly diagonal in the common basis $\{|ns,\pm\rangle\}$, moreover they do not depend on spin state. In order to represent the interaction (fig. 1.3) we can plot V^{ns} which is the KHe pair interaction (in the unrotated frame) and $E^{nl}_{ss\alpha\alpha}$ which is the averaged potential: it represents the potential felt by a diabatically displaced K, this actually gives a snapshot of the system at $t = 0$. We will discuss in section 2.1.1 the meaning of adiabatic *vs* diabatic hypothesis and their reliability.

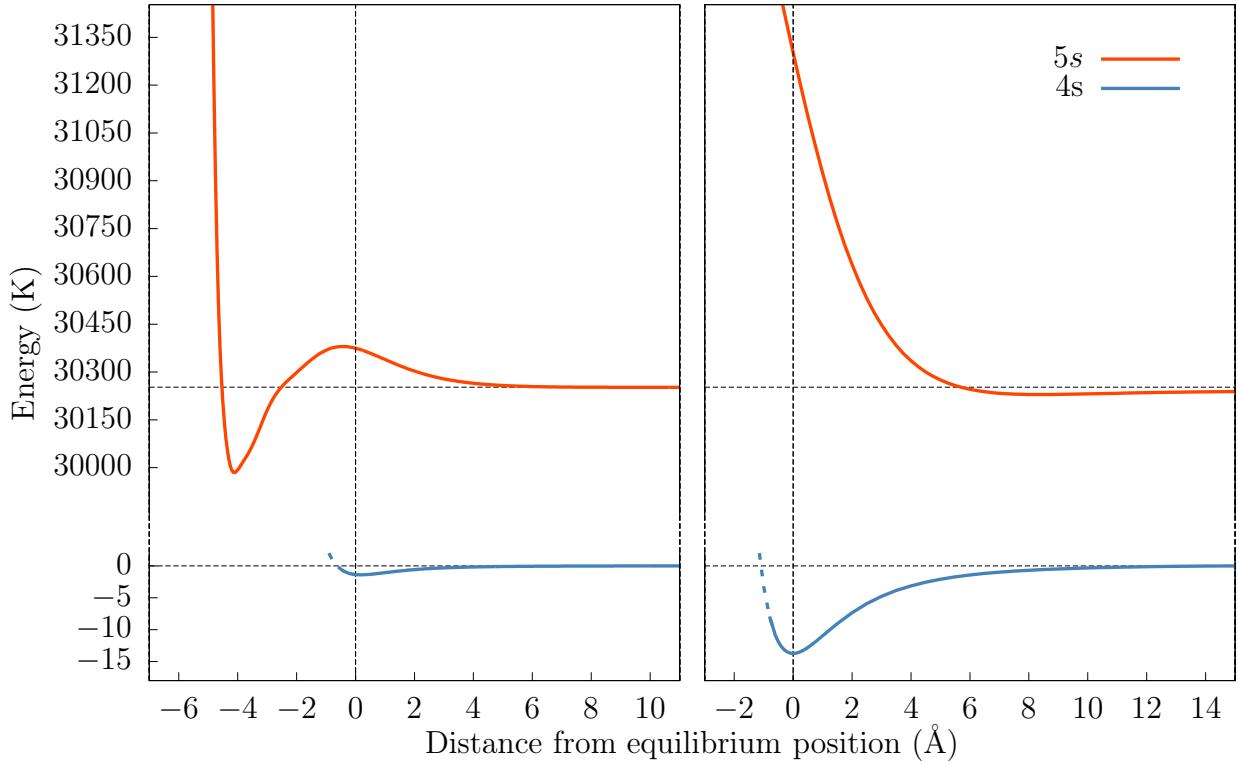

Figure 1.3 – Pair potential (left) and averaged interaction over the droplet (right). Equilibrium distances: $r = 7.0$ Å for KHe and $r = 26.3$ Å (between centers of mass) for KHe_{1000}

An in-depth description with the $(4p)$ state

The $(4p)$ state is more involved since it corresponds to $L = 1$: on the one hand it no longer has spherical symmetry but cylindrical symmetry, and on the other hand spin-orbit coupling has to be taken into account. Let us first focus on the electrostatic interaction.

$$\begin{aligned} U^{4p/\mathrm{ES}}_{ij\alpha\beta}(\mathbf{r}_m) &= \langle i,\alpha|\,\mathcal{R}_m^{-1} H^{4p/\mathrm{ES}}_{\mathrm{K-He}}(\mathbf{r}_m)\,\mathcal{R}_m\,|j,\beta\rangle \\ &= \langle i,\alpha|\,\mathcal{R}_m^{-1}\left(V^{4p}_\Pi(\mathbf{r}_n)\,\mathbb{I}_3 + [V^{4p}_\Sigma(\mathbf{r}_n) - V^{4p}_\Pi(\mathbf{r}_n)]\,|p_{z_n}\rangle\,\langle p_{z_n}|\right)\,\mathcal{R}_m\,|j,\beta\rangle \\ &= \langle i,\alpha|\left(V^{4p}_\Pi(\mathbf{r}_n)\,\mathbb{I}_3 + [V^{4p}_\Sigma(\mathbf{r}_n) - V^{4p}_\Pi(\mathbf{r}_n)]\{\mathcal{R}_m^{-1}\,|p_{z_n}\rangle\,\langle p_{z_n}|\,\mathcal{R}_m\}\right)\,|j,\beta\rangle \qquad (1.25) \\ &= \left(V^{4p}_\Pi(\mathbf{r}_n)\,\delta_{ij} + [V^{4p}_\Sigma(\mathbf{r}_n) - V^{4p}_\Pi(\mathbf{r}_n)]\,\langle i|\,\mathcal{R}_m^{-1}\,|p_{z_n}\rangle\,\langle p_{z_n}|\,\mathcal{R}_m\,|j\rangle\right)\,\delta_{\alpha\beta} \qquad (1.26) \end{aligned}$$

Expressing the interaction in a set of real orbitals makes the expression of the rotation easier because they transform as $\mathbb{R}^3$ vectors

$$\langle i|\,\mathcal{R}_m^{-1}\,|p_{z_m}\rangle\,\langle p_{z_m}|\,\mathcal{R}_m\,|j\rangle = \frac{x_m^i\,x_m^j}{\|\mathbf{r}_m\|^2} \tag{1.27}$$

We can then write the electrostatic matrix elements

$$U_{ij\alpha\beta}^{4p/\mathrm{ES}}(\mathbf{r}_m) = \left(V_\Pi(\mathbf{r}_m)\,\delta_{ij} + [V_\Sigma(\mathbf{r}_m) - V_\Pi(\mathbf{r}_m)]\,\frac{x_m^i\,x_m^j}{\|\mathbf{r}_m\|^2}\right)\,\delta_{\alpha\beta} \tag{1.28}$$

$$E_{ij\alpha\beta}^{4p/\mathrm{ES}}(\mathbf{r}_\mathrm{K}) = \int \mathrm{d}\mathbf{r}\,\rho(\mathbf{r}+\mathbf{r}_\mathrm{K})\,\left(V_\Pi(\mathbf{r})\,\delta_{ij} + [V_\Sigma(\mathbf{r}) - V_\Pi(\mathbf{r})]\,\frac{x^i\,x^j}{\|\mathbf{r}\|^2}\right)\,\delta_{\alpha\beta} \tag{1.29}$$

Diagonalizing the electrostatic Hamiltonian within cylindrical symmetry[1] gives a set of eigenvalues $\{\varepsilon\}$

$$\begin{aligned}\varepsilon_i(\mathbf{r}_\mathrm{K}) = E_{ii\alpha\alpha}^{4p/\mathrm{ES}}(\mathbf{r}_\mathrm{K}) = 2\pi \iint r^2\sin\theta\,\mathrm{d}\theta\,\mathrm{d}r\;\rho\left(\sqrt{|r^2+r_\mathrm{K}^2+2rr_\mathrm{K}\cos\theta|}\right)\\ \left(V_\Pi(r) + [V_\Sigma(r) - V_\Pi(r)]\,\left[\frac{1}{2}(\delta_{ip_x}+\delta_{ip_y})\sin^2\theta + \delta_{ip_z}\cos^2\theta\right]\right)\end{aligned} \tag{1.30}$$

Because of the overall cylindrical symmetry we see that the Hamiltonian is diagonal in the common basis. In particular the associated eigenvectors are the real $4p$-orbitals $\{|4p_x,\pm\rangle\,,|4p_y,\pm\rangle\,,|4p_z\rangle\,,\pm\}$[2] and Λ is a good quantum number.

We now turn to the spin-orbit interaction in the same basis set, which is known as the *uncoupled* basis set: $\{|p_x,+\rangle\,,|p_x,-\rangle\,,|p_y,+\rangle\,,|p_y,-\rangle\,,|p_z,+\rangle\,,|p_z,-\rangle\}$. The matrix elements of the spin-orbit Hamiltonian are more easily expressed in the basis set of (complex) orbitals with a well defined value of Λ, and then transformed back to the real (cartesian) orbitals. We end up with

$$H^{4p/\mathrm{SO}} = A_\mathrm{LS}\,\mathbf{L}\cdot\mathbf{S} = A_\mathrm{LS}\,(L_+S_- + L_-S_+ + L_zS_z) = \frac{A_\mathrm{LS}}{2}\begin{pmatrix} 0 & 0 & -i & 0 & 0 & 1\\ 0 & 0 & 0 & i & -1 & 0\\ i & 0 & 0 & 0 & 0 & -i\\ 0 & -i & 0 & 0 & -i & 0\\ 0 & -1 & 0 & i & 0 & 0\\ 1 & 0 & i & 0 & 0 & 0\end{pmatrix} \tag{1.31}$$

The matrix elements of the full Hamiltonian are then

$$U_{ij\alpha\beta}^{4p}(\mathbf{r}_m) = U_{ij\alpha\beta}^{4p/\mathrm{ES}}(\mathbf{r}_m) + U_{ij\alpha\beta}^{4p/\mathrm{SO}} \tag{1.32}$$

$$E_{ij\alpha\beta}^{4p}(\mathbf{r}_\mathrm{K}) = \int \mathrm{d}\mathbf{r}\,\rho(\mathbf{r}+\mathbf{r}_\mathrm{K})\,\left(V_\Pi(\mathbf{r})\,\delta_{ij} + [V_\Sigma(\mathbf{r}) - V_\Pi(\mathbf{r})]\,\frac{x^i\,x^j}{\|\mathbf{r}\|^2}\right)\,\delta_{\alpha\beta} + U_{ij\alpha\beta}^{4p/\mathrm{SO}} \tag{1.33}$$

$$\tag{1.34}$$

[1] The ground state helium droplet being spherical, the ground state for K-He$_N$ has cylindrical symmetry, and this symmetry is conserved upon excitation.

[2] Note that these states are actually doubly degenerate because of spin degeneracy

Its diagonalization gives the set of eigenvalues $\{\xi\}$

$$\begin{aligned}
\xi_1(\mathbf{r}_K) &= \frac{1}{2}(\varepsilon_1+\varepsilon_3) + \frac{1}{4}\left(-A_{LS} + \sqrt{9A_{LS}^2 - 4A_{LS}(\varepsilon_1-\varepsilon_3) + 4(\varepsilon_1-\varepsilon_3)^2}\right) \\
\xi_2(\mathbf{r}_K) &= \varepsilon_1 + \frac{A_{LS}}{2} \\
\xi_3(\mathbf{r}_K) &= \frac{1}{2}(\varepsilon_1+\varepsilon_3) + \frac{1}{4}\left(-A_{LS} - \sqrt{9A_{LS}^2 - 4A_{LS}(\varepsilon_1-\varepsilon_3) + 4(\varepsilon_1-\varepsilon_3)^2}\right)
\end{aligned} \tag{1.35}$$

	ξ_1	ξ_2	ξ_3
Value when $\varepsilon_i \ll A_{LS}$	$+\frac{A_{LS}}{2}$	$+\frac{A_{LS}}{2}$	$-A_{LS}$
Associated J value	3/2	3/2	1/2
Value when $\varepsilon_i \gg A_{LS}$	ε_3	ε_1	ε_1
Associated $\lvert\Lambda\rvert$ value	0	1	1
Associated $\lvert\Omega\rvert$ value	1/2	3/2	1/2
Label	$\Sigma_{1/2}$	$\Pi_{3/2}$	$\Pi_{1/2}$

Table 1.1 – Determination of true good quantum number Ω and approximate ones Λ and J

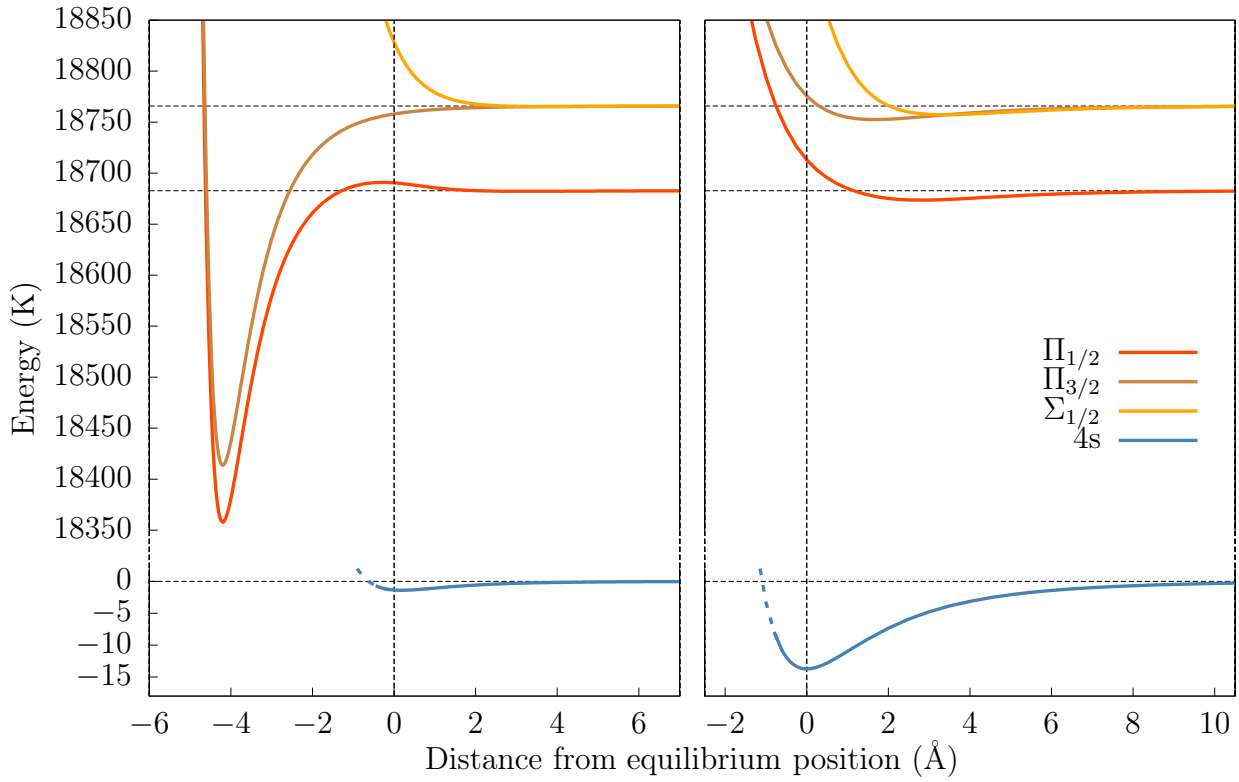

Figure 1.4 – Pair potential (left) and averaged interaction over the droplet (right)

We present in table 1.1 the reasoning used to determine the true good quantum number Ω and the approximate ones: Λ and J. We use the following label Λ_Ω for energy states. J does not appear because in the excitation region the $\Sigma - \Pi$ splitting between electrostatic eigenvalues is larger that

the atomic spin-orbit splitting, such that Λ gives a better representation of the reality.

In the same way than for the $(5s)$ state (fig. 1.3), we plot both the pair interaction and the averaged potential in fig. 1.4. Keep in mind that pair potential refers to the unrotated basis, for instance in a global $\Pi_{1/2}$ state, there are only the helium in the internuclear axis that interact with $\Pi_{1/2}$ potential. Note also that the averaged potential corresponds to one of the ξ value labeled according to the previous discussion.

1.2.4 Writing energy contribution to doped helium droplet

In order to describe the electronic degree of freedom, we introduce the electronic wave function $|\lambda\rangle$

$$|\lambda\rangle = \sum_{\substack{\alpha=\{+,-\} \\ i\in\{nl\,\text{orbitals}\}}} \lambda_{i\alpha}\,|i,\alpha\rangle \tag{1.36}$$

Let us consider the interaction Hamiltonian for $H^{nl}_{\mathrm{K-He}_N}(\mathbf{r}_\mathrm{K})$ (eq. 1.18), we will write the corresponding interaction in the continuum formalism. We first describe the total energy for a point-like interaction, *id est* a classical particle

$$E[\rho] \to E[\rho,\mathbf{r}_\mathrm{K},\lambda] = E[\rho] + \langle\Psi,\lambda|\,H^{nl}_{\mathrm{K-He}_N}(\mathbf{r}_\mathrm{K})\,|\Psi,\lambda\rangle \tag{1.37}$$

The interaction part is given by

$$\langle\Psi,\lambda|\,H^{nl}_{\mathrm{K-He}_N}\,|\Psi,\lambda\rangle = \int \mathrm{d}\mathbf{r}\;\rho(\mathbf{r}+\mathbf{r}_\mathrm{K})\,\langle\lambda|\,\mathcal{R}^{-1}(\mathbf{r})H^{nl/\mathrm{ES}}_{\mathrm{K-He}}(\mathbf{r})\,\mathcal{R}(\mathbf{r})\,|\lambda\rangle + \langle\lambda|\,H^{nl/\mathrm{SO}}\,|\lambda\rangle \tag{1.38}$$

$$\equiv \int \mathrm{d}\mathbf{r}\;\rho(\mathbf{r})\,V^{nl\lambda}_{\mathrm{K-He}}(\mathbf{r}-\mathbf{r}_\mathrm{K}) + \langle\lambda|\,H^{nl/\mathrm{SO}}\,|\lambda\rangle \tag{1.39}$$

where the time evolution of the *effective* potential is given by that of the electronic wave packet $|\lambda\rangle$, using notation of eq. 1.28

$$V^{nl\lambda}_{\mathrm{K-He}}(\mathbf{r}) = \langle\lambda|\,\mathcal{R}^{-1}(\mathbf{r})H^{nl/\mathrm{ES}}_{\mathrm{K-He}}(\mathbf{r})\,\mathcal{R}(\mathbf{r})\,|\lambda\rangle = \sum_{ij\alpha\beta}\lambda^*_{i\alpha}\,U^{nl/\mathrm{ES}}_{ij\alpha\beta}(\mathbf{r})\,\lambda_{j\beta} \tag{1.40}$$

For a quantum particle described by a wave function ϕ, eq. 1.37 becomes

$$E[\rho] \to E[\rho,\phi,\lambda] = E[\rho] + \langle\Psi,\lambda,\phi|\,H^{nl}_{\mathrm{K-He}_N}(\mathbf{r}_\mathrm{K})\,|\Psi,\lambda,\phi\rangle \tag{1.41}$$

In the classical case, variation of the total energy with respect to the effective helium wave function (order parameter) Ψ gives the Euler-Lagrange equations.

$$E[\rho,\mathbf{r}_\mathrm{K},\lambda] = E[\rho] + \int \mathrm{d}\mathbf{r}\;\rho(\mathbf{r})V^{nl\lambda}_{\mathrm{K-He}}(\mathbf{r}-\mathbf{r}_\mathrm{K}) + \langle\lambda|\,H^{nl/\mathrm{SO}}\,|\lambda\rangle \tag{1.42}$$

$$\Rightarrow \left(-\frac{\hbar^2}{2m_\mathrm{K}}\boldsymbol{\nabla}^2 + \frac{\delta\mathcal{E}_c}{\delta\rho} + V^{nl\lambda}_{\mathrm{K-He}}(\mathbf{r}-\mathbf{r}_\mathrm{K})\right)\Psi(\mathbf{r}) = \mu\Psi(\mathbf{r}) \tag{1.43}$$

In the quantum case one adds variation with respect to the alkali wave function, which yields two coupled equations

$$E[\rho,\phi,\lambda] = E[\rho] + \iint \mathrm{d}\mathbf{r}\,\mathrm{d}\mathbf{r}_\mathrm{K}\ \rho(\mathbf{r}) V^{nl\lambda}_{\mathrm{K-He}}(\mathbf{r}-\mathbf{r}_\mathrm{K})|\phi(\mathbf{r}_\mathrm{K})|^2 + \frac{\hbar^2}{2m_\mathrm{K}}\int \mathrm{d}\mathbf{r}_\mathrm{K}\,|\boldsymbol{\nabla}_{\mathbf{r}_\mathrm{K}}\phi(\mathbf{r}_\mathrm{K})|^2 + \langle\lambda|\,H^{nl/\mathrm{SO}}\,|\lambda\rangle \tag{1.44}$$

$$\Rightarrow \begin{cases} \left(-\frac{\hbar^2}{2m_\mathrm{He}}\boldsymbol{\nabla}^2_\mathbf{r} + \frac{\delta\mathcal{E}_c}{\delta\rho} + \int \mathrm{d}\mathbf{r}_\mathrm{K}\ V^{nl\lambda}_{\mathrm{K-He}}(\mathbf{r}-\mathbf{r}_\mathrm{K})|\phi(\mathbf{r}_\mathrm{K})|^2\right)\Psi(\mathbf{r}) = \mu\Psi(\mathbf{r}) \\ \left(-\frac{\hbar^2}{2m_\mathrm{K}}\boldsymbol{\nabla}^2_{\mathbf{r}_\mathrm{K}} + \int \mathrm{d}\mathbf{r}\ V^{nl\lambda}_{\mathrm{K-He}}(\mathbf{r}-\mathbf{r}_\mathrm{K})\rho(\mathbf{r})\right)\phi(\mathbf{r}_\mathrm{K}) = \varepsilon\phi(\mathbf{r}_\mathrm{K}) \end{cases} \tag{1.45}$$

We see that thanks to the introduction of the *order parameter* these equations look like SCHRODINGER equations. Technical details on how to solve these equations are given in the annex a.

1.3 TDDFT

The purpose of this work is to study the dynamic evolution of our system under absorption of a photon. Hence in this section we describe the method used for the dynamics. It is based on the RUNGE-GROSS theorem [30] which extends the DFT formalism to time dependent studies (TD-DFT).

1.3.1 Excitation process

We assume that the exciting laser pulse is very short, so that the nuclei do not have time to move ("vertical transition"). This amounts to considering that the initial conditions for the dynamics are the ground equilibrium helium density and alkali position for the nuclei, and that the electronic state is suddenly switched to the excited state $(4p)$ or $(5s)$. In other words, we start a dynamic study with a new interaction Hamiltonian but with the ground state density, this is equivalent to the FRANCK-CONDON approximation with a constant transition dipole moment.

1.3.2 Classical dynamics

TD-DFT is based on the variation of the action $\mathcal{A}$ (instead of energy in DFT) with respect to all its parameters

$$\mathcal{A}[\Psi,\mathbf{r}_\mathrm{K},\lambda] = \int \mathrm{d}t\left(E[\Psi,\mathbf{r}_\mathrm{K},\lambda] - i\hbar\int \mathrm{d}\mathbf{r}\,\Psi^*(\mathbf{r},t)\frac{\partial}{\partial t}\Psi(\mathbf{r},t) - i\hbar\,\langle\lambda|\,\frac{\partial}{\partial t}\,|\lambda\rangle - \frac{1}{2}m_\mathrm{K}\dot{\mathbf{r}}^2_\mathrm{K}\right) \tag{1.46}$$

This procedure yields to a set of three coupled equations that govern the dynamics (computational details are described in the annex b).

$$i\hbar\frac{\partial}{\partial t}\Psi(\mathbf{r},t) = \left(-\frac{\hbar^2}{2m_\mathrm{He}}\boldsymbol{\nabla}^2_\mathbf{r} + \frac{\delta\mathcal{E}_c}{\delta\rho(\mathbf{r})} + V^{nl\lambda}_{\mathrm{K-He}}(\mathbf{r}-\mathbf{r}_\mathrm{K})\right)\Psi(\mathbf{r},t) \tag{1.47}$$

$$i\hbar\frac{\partial}{\partial t}\,|\lambda\rangle = H^{nl}_{\mathrm{K-He}_N}(\mathbf{r}_\mathrm{K})\,|\lambda\rangle \tag{1.48}$$

$$m_\mathrm{K}\ddot{\mathbf{r}}_\mathrm{K} = -\boldsymbol{\nabla}_{\mathbf{r}_\mathrm{K}}\left(\int \mathrm{d}\mathbf{r}\,\rho(\mathbf{r})V^{nl\lambda}_{\mathrm{K-He}}(\mathbf{r}-\mathbf{r}_\mathrm{K})\right) = -\left(\int \mathrm{d}\mathbf{r}\,V^{nl\lambda}_{\mathrm{K-He}}(\mathbf{r}-\mathbf{r}_\mathrm{K})\boldsymbol{\nabla}_\mathbf{r}\rho(\mathbf{r})\right) \tag{1.49}$$

1.3.3 Test particles and quantum dynamics in an isotrotropic state

We could use the same procedure as for treating K quantum mechanically in the statics. However, the potassium atom can acquire a rather high kinetic energy when dissociating, and this is impossible to describe with the same grid as that of the helium density. Instead we used a test particles method based on Bohmian dynamics, as proposed by Hernando *et al.* [16] for Li and Na photodissociation from a helium droplet.

The starting point is to write the impurity complex wave function in the exponential with modulus $\psi(\mathbf{r},t)$ and phase $\mathcal{S}(\mathbf{r},t)$, ψ and $\mathcal{S}$ being two real and positive functions

$$\phi(\mathbf{r},t) = \psi(\mathbf{r},t)\,\mathrm{e}^{i\mathcal{S}(\mathbf{r},t)/\hbar} \tag{1.50}$$

We set $\mathbf{v} = \frac{1}{m_\mathrm{K}}\boldsymbol{\nabla}\mathcal{S}$, then the current density $\mathbf{j} = \frac{\hbar}{2m_\mathrm{K}}\left(\phi^*\boldsymbol{\nabla}\phi - \phi\boldsymbol{\nabla}\phi^*\right)$ becomes $\mathbf{j} = \psi^2\,\mathbf{v}$. Finally the SCHRÖDINGER equation gives a coupled system of equations

$$\frac{\partial\psi^2(\mathbf{r},t)}{\partial t} = -\boldsymbol{\nabla}\cdot\mathbf{j}(\mathbf{r},t) \tag{1.51}$$

$$-\frac{\partial\mathcal{S}(\mathbf{r},t)}{\partial t} = \frac{1}{2}m_\mathrm{K}\mathbf{v}^2(\mathbf{r},t) + \mathcal{Q}(\mathbf{r},t) + V(\mathbf{r}) \quad \text{with} \quad \mathcal{Q} = -\frac{\hbar^2}{2m_\mathrm{K}}\frac{\boldsymbol{\nabla}^2\psi}{\psi} \tag{1.52}$$

Then, we consider a set of M particles with trajectories $\{\mathbf{R_j}(t)\}$ with $\mathbf{R}_i(t) = \mathbf{R}(\mathbf{r}_i,t)$ and $\mathbf{R}_i(0) = \mathbf{r}_i$ such that

$$\psi(\mathbf{r},t) = \lim_{M\to\infty}\sum_{i=1}^{M}\delta[\mathbf{r}-\mathbf{R}_i(t)] \tag{1.53}$$

$$\mathbf{j}(\mathbf{r},t) = \lim_{M\to\infty}\sum_{i=1}^{M}\mathbf{v}[\mathbf{R_i}(t)]\delta[\mathbf{r}-\mathbf{R}_i(t)] \tag{1.54}$$

It can be shown [31] that eq. 1.51 is equivalent to $\dot{\mathbf{R}}_i(t) = \mathbf{v}[\mathbf{R}_i(t)]$. Then by taking the gradient of eq. 1.52 and rewriting it in the Lagrangian reference frame ($\mathrm{d}/\mathrm{d}t = \partial/\partial t + \mathbf{v}\cdot\nabla$) one obtains the *quantum* NEWTON equation

$$m\,\ddot{\mathbf{R}}_i(t) = -\nabla[\mathcal{Q}(\mathbf{r},t) + V(\mathbf{r},t)]|_{\mathbf{r}=\mathbf{R}_i(t)} \tag{1.55}$$

In practical, we use $M = 2\times10^5$ test particles, we randomly generate their initial position using the ground state wave function and then we solve for each its NEWTON equation (in the same way as in the previous dynamics equations, see the annex b). In order to compute physical quantities and the so-called quantum potential $\mathcal{Q}$, one builds a 3D histogram based on our simulation grid with test particle positions at the given time. In particulary one can show [31] the following equations for potassium position, velocity and kinetic energy expected values

$$\langle\phi|\,\mathbf{r}\,|\phi\rangle = \int\mathrm{d}\mathbf{r}\,\mathbf{r}\,\psi^2(\mathbf{r},t) \tag{1.56}$$

$$\langle\phi|\,\mathbf{v}\,|\phi\rangle = \frac{1}{m}\int\mathrm{d}\mathbf{r}\,\mathbf{j}(\mathbf{r},t) \tag{1.57}$$

$$\langle\phi|-\frac{\hbar^2\nabla^2}{2m_\mathrm{K}}|\phi\rangle = \int\mathrm{d}\mathbf{r}\left[\frac{1}{2}m\mathbf{v}^2(\mathbf{r},t) + \mathcal{Q}(\mathbf{r},t)\right]\psi^2(\mathbf{r},t) \tag{1.58}$$

2. Simulation

We will now describe and discuss the results of our simulations. For the whole study we used a number $N = 1000$ of helium atoms. It is a compromise between realistic size to compare with experiments (typical droplet sizes between ~ 500 and ~ 10000 atoms for this type of measurements) and computational cost.

2.1 Finding ground state properties

$(4s)$ state is the ground state of our system. Thanks to the moderate computational cost of its simulation we can examine several important factors. The first one is the comparison of a classical *vs* quantum treatment of the potassium atom. The second one is the version of the functional used, the original OT one or a modification designed to deal with high values of the density described as solid functional in section 1.1.2.

2.1.1 Quantum versus classical potassium

The ground state K wave function is expected to be smooth. Hence it can be described using the same grid as the helium one. As can be seen in fig. 2.1, a quantum treatment of the potassium atom leads to a slightly displaced atom from center of mass of the droplet (around 1Å) compared to the position given by a classical description. In addition, the droplet radius is slightly increased and the surface region slightly more diffuse. This phenomenon can be understood by considering the spatial extension of the impurity wave-function compared to the classical point-like position.

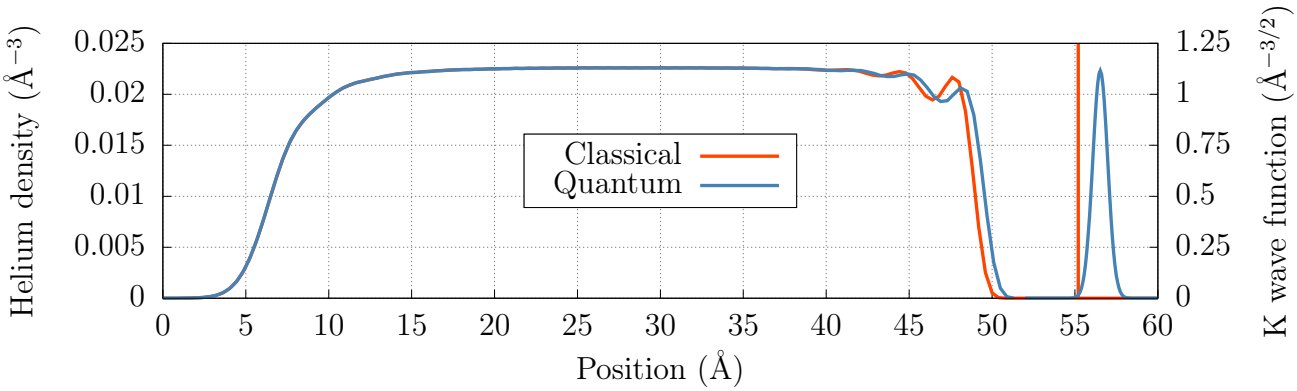

Figure 2.1 – Density profile in a plane containing the center of mass of the droplet and the potassium atom, for a quantum or a classical description of K

2.1.2 Quick discussion on the influence of the version of the functional

We already discussed the fact that the OTC functional could become unstable during a dynamics simulation due to the fact that it cannot handle sharp features appearing around attractive dopants. This can occur in the excited $(4p)$ states because of the attractive Π well. The two versions can be compared in the static study of the ground $(4s)$ state. We see in fig. 2.2 that the two functionals

give nearly the same helium density, except near the dopant where the solid version gives a smoother profile, as expected.

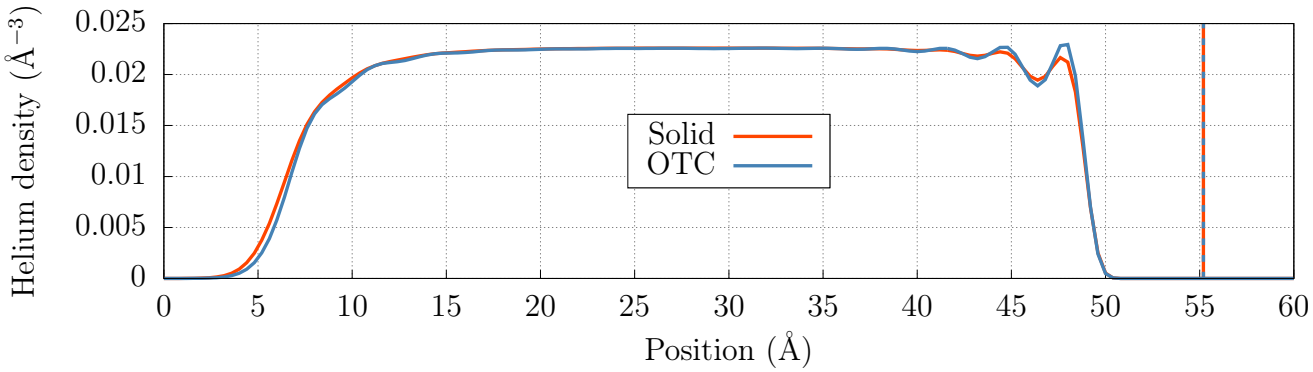

Figure 2.2 – Density profile in a plane containing the center of mass of the droplet and the potassium atom, for the solid or the OTC functional

2.1.3 Justifying diabatic hypothesis

One model that has been very much used to interpret experimental spectra of alkali atoms bound to helium droplets or even some of the dynamics aspects of their photodissociation is the so-called *pseudo-diatomic model*. In this model the system is represented as a diatomic molecule in which the helium droplet plays the role of a pseudo-atom. The potential energy curves for this model are then taken by averaging the pair potentials over the (static) helium density.

There are two ways of choosing which density to use for this convolution. The first one is what we call the *diabatic* hypothesis: the motion of K is supposed to be much faster than the droplet one. The second one, which will be called *adiabatic*, optimizes the helium density for each value of the position of the dopant, which is equivalent to assuming that the helium density can adapt instantly to a new position of the potassium. We use here the simple case of the ground ($4s$) study to get an idea of which hypothesis is closer to reality. Let us stress that both models imply that there is no energy exchange between the dopant and the droplet during the dynamics, whereas in the TDDFT description the whole dynamics is described, albeit in a mean-field way.

Our formalism (minimization of a functional with respect to all its parameters) makes it possible to add constraints to our minimization. We can thus impose a given distance $\mathcal{Z}_0$ between the dopant and the helium center of mass (the actual distance is noted $\mathcal{Z}$)

$$E[\rho] \to E[\rho, \mathcal{Z}_0] = E[\rho] + \frac{\alpha}{2}(\mathcal{Z} - \mathcal{Z}_0)^2 \quad \text{with } \alpha \text{ an arbitrary constant} \tag{2.1}$$

Then we proceed in the following way: we start simulations with different $\mathcal{Z}_0$ value and we register the first and last energy balance. The first one give the system energy without relaxation (diabatic approximation) while the final one gives the energy after minimization (adiabatic approximation). In order to decide which of the two approximations is better to describe our system we can compare the results to the DFT simulation with a quantum description of K, which is expected to be more accurate. The idea is to consider that in the ground state the particle is locally feeling a harmonic potential, so we can use the well known ground state wave function and associated energy.

$$\psi_0(z) = \left(\frac{\alpha}{\pi}\right)^{1/4} \mathrm{e}^{-\alpha z^2/2} \quad \text{and} \quad E_0 = \frac{\hbar\omega}{2} \quad \text{with} \quad \alpha = \frac{m\omega}{\hbar} \tag{2.2}$$

The results are shown in fig. 2.3. First we can note that the diabatic and adiabatic potentials do not reach the same asymptotic energy. This is because in the adiabatic approximation the helium droplet is a pure, relaxed helium droplet while in the diabatic one it has the same density as when the potassium was at equilibrium distance. Second, we observe that the quantum case (DFT with quantum description of K) seems to be closer to the diabatic approximation.

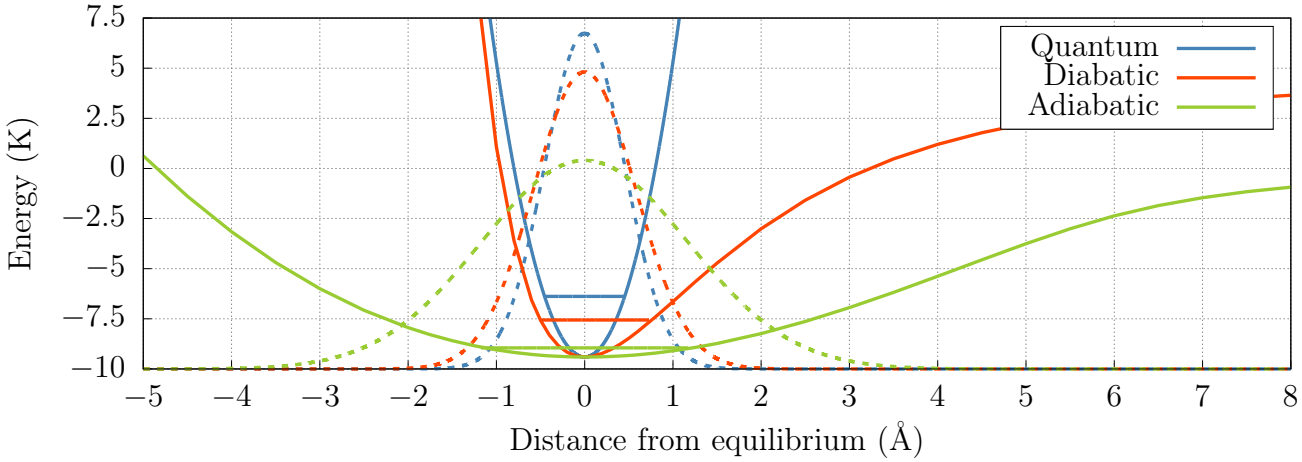

Figure 2.3 – Diabatic, adiabatic and quantum potentials with associated wave functions and zero point energies in the harmonic approximation. The quantum potential is deduced from a harmonic fit of the wave function obtained from DFT with K treated quantum mechanically; the diabatic and adiabatic wave functions are obtained from a harmonic fit of the corresponding potentials

2.2 Classical dynamics towards ($4p$) states

The ground state properties being established, we will now present the dynamics simulation of the KHe_N system under a $4p \leftarrow 4s$ photo-excitation. As already discussed, the $4p$ state is split by interaction with helium and by spin-orbit coupling. Hence we will present the dynamics following each of the three $\Pi_{1/2}$, $\Pi_{3/2}$ and $\Sigma_{1/2}$ excitations.

2.2.1 Quantum versus classical spectra

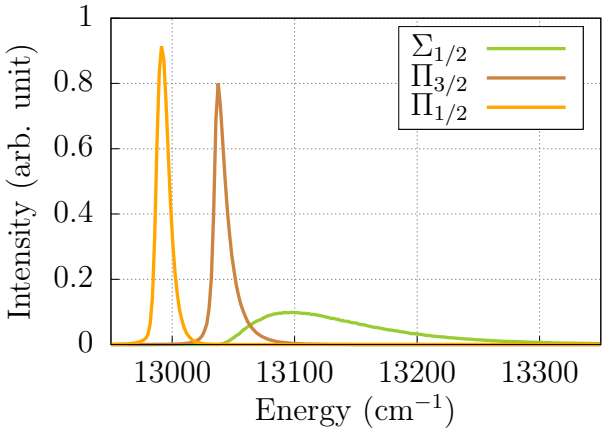

Figure 2.4 – $4p \rightarrow 4s$ absorption spectra with different state contributions for quantum K

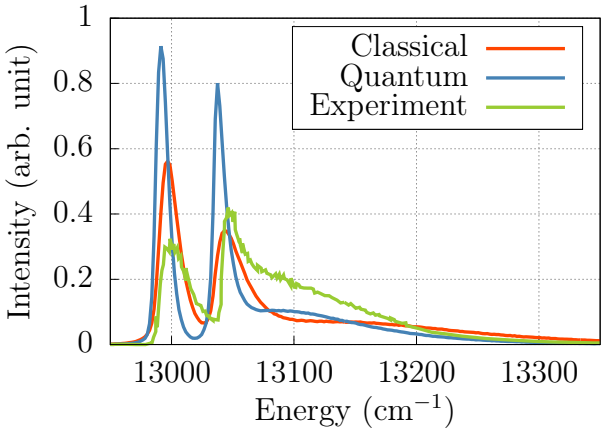

Figure 2.5 – Comparisons between quantum, classical and experimental spectra [12]

The programs are not yet prepared to describe the quantum motion of K in an anisotropic state. However, we can still use the quantum ground state density to simulate the spectra with the method described in the annex c. This gives the only opportunity to judge the classical hypothesis for K motion by comparing this spectra to experimental data from [12].

We clearly see that both the classical and the quantum spectra give a very good agreement. However, they fail to describe the relative intensity of the two main peaks and they underestimate the $\Sigma_{1/2}$ component. We can conclude that the classical spectrum is really close to the quantum one and to the experimental data, which justifies our hypothesis and validates the potentials used.

2.2.2 $\Sigma_{1/2}$ excitation: leaving free potassium

We start our dynamics study with the $\Sigma_{1/2}$ excitation. We observe in fig. 2.8 a fast ejection of the K atom in approximatively 0.2 ps. This behavior could be predicted from fig. 1.4, because the averaged interaction is repulsive, however we have to be cautious because this only gives a snapshot of the energy profile at $t = 0$ since the droplet is not rigid and can absorb energy from K.

We note in fig. 2.6 the global deformation of the droplet during ejection and the creation of density waves in the droplet.

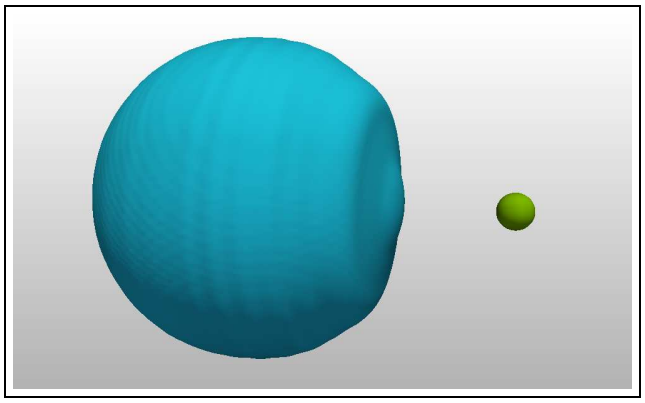

Figure 2.6 – Snapshot of He_N density and leaving K at $t = 8.5$ ps

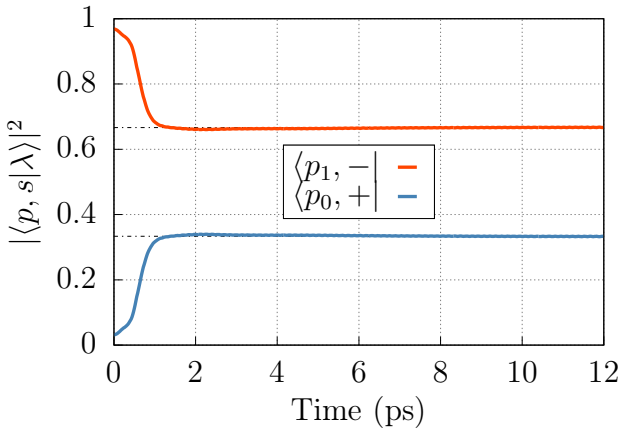

Figure 2.7 – Evolution of the electronic state as a function of time

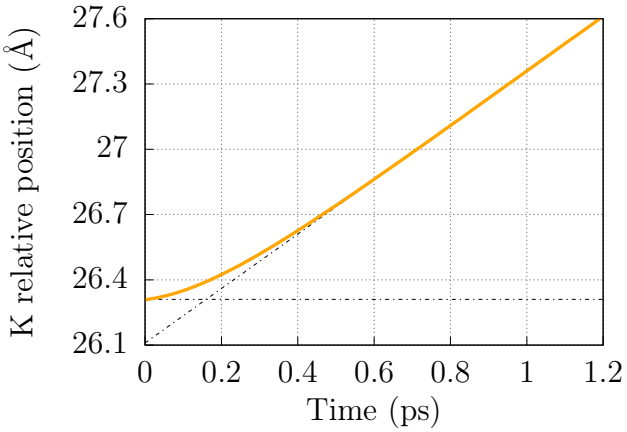

Figure 2.8 – Distance between K and He_N centers of mass as a function of time

The study of the evolution of the internal electronic state will be important in following discussions, this is why we start discussing it for $\Sigma_{1/2}$ as a simple case. We saw in section 1.2.2 that Ω is the only true good quantum number. Here we have $\Omega = 1/2$[1]. This can be checked in fig. 2.7 since it is a linear combination of $|p_1, -\rangle$ and $|p_0, +\rangle$. In addition we have seen that Λ should be a good quantum number in the excitation region (section 1.2.2). For the $\Sigma_{1/2}$ state $\Lambda \approx 0$, which is why $|p_0, +\rangle$ is

[1]We only discuss the positive case but the reasoning is the same for $\Omega = -1/2$ since they are degenerate

dominant at $t = 0$. Finally we can see that once K is far from droplet, its internal state becomes an eigenvector of $\mathbf{J}^2$ with eigenvalue $J = 3/2$. This is also expected because J is a good quantum number in this region and the $\Sigma_{1/2}$ state connects asymptotically to $J = 3/2$ (section 1.2.3)

$$|\lambda\rangle \underset{t\to\infty}{\longrightarrow} |J = 3/2, \Omega = 1/2\rangle = \sqrt{\frac{1}{3}}\,|p_1, -\rangle + \sqrt{\frac{2}{3}}\,|p_0, +\rangle \tag{2.3}$$

2.2.3 $\Pi_{1/2}$ excitation: complexity arises

Bouncing potassium

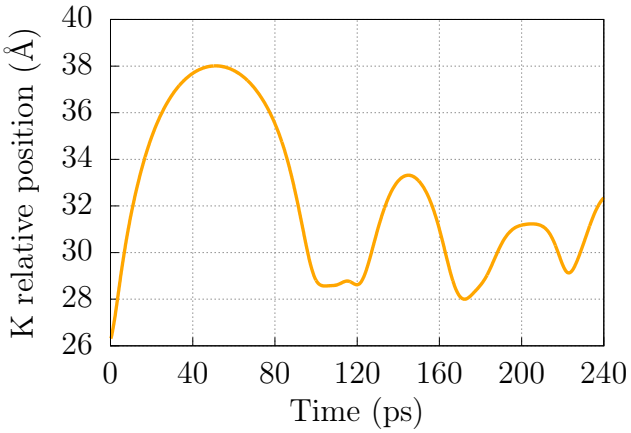

Figure 2.9 – Distance between K and He_N centers of mass as a function of time

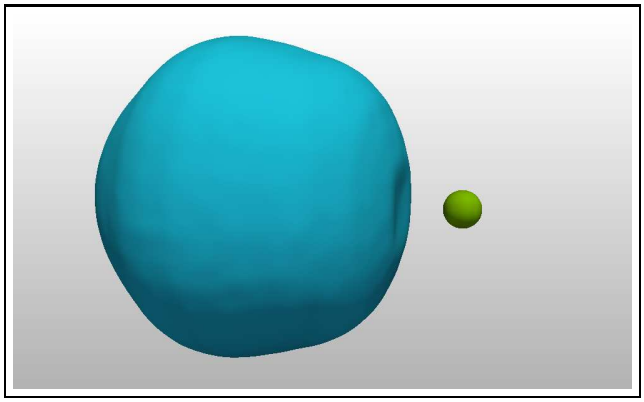

Figure 2.10 – Snapshot of He_N density and bouncing K at $t = 182$ ps

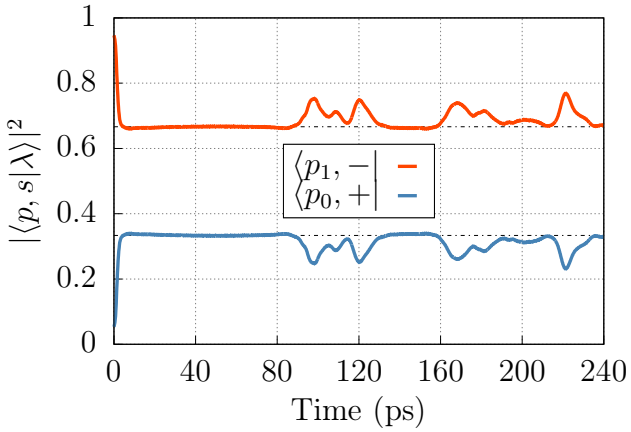

Figure 2.11 – Evolution of the electronic state as a function of time

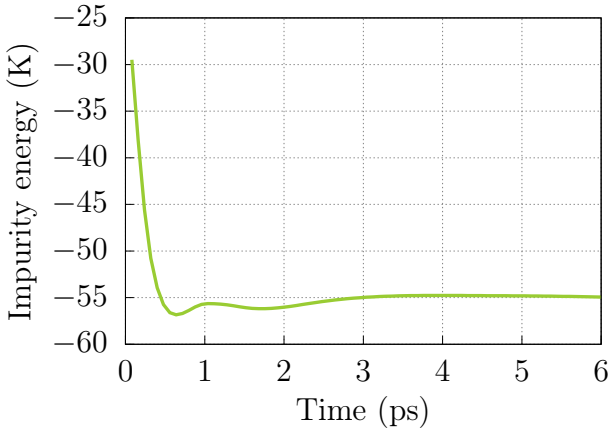

Figure 2.12 – Total potassium energy as a function of time

After excitation to the $\Pi_{1/2}$ state the potassium does not leave the droplet as can be seen in fig. 2.9. Moreover the 3D snapshot fig. 2.10 shows no exciplex formation. This behavior can look surprising at first because the pair potential is repulsive and the averaged potential shows that K has enough potential energy at $t = 0$ to dissociate (cf fig. 1.4). One can actually easily understand what is going on by plotting the total impurity energy as a function of time. As shown in fig. 2.12, K is giving a lot of energy to the droplet: up to 25 K. On the other hand the $\Pi_{1/2}$ pair potential has a tiny well about +4.0 Å away from the initial position, which creates both a long range attraction and a barrier when the particle is coming back. These two phenomena explain why we have a bouncing-bound K. In particular we see that the bouncing occurs at around +2.5 Å, which is consistent with the previous

explanation. One can also understand why there is no exciplex formation: the deep well in the pair potential is not accessible due to the tiny barrier.

The electronic state evolution for $\Pi_{1/2}$ excitation is presented in fig. 2.11. The situation is similar to that of $\Sigma_{1/2}$ excitation because $\Omega = 1/2$, but here $\Lambda \approx 1$ and $J \approx 1/2$ so that $|p_1, -\rangle$ is dominant at small distance and we find $|J = 1/2, \Omega = 1/2\rangle$ at large distances. In particular we note that when K is bouncing we are in an intermediate case.

Displacing the excitation position

The previous discussion showed that the tiny barrier close to the excitation region plays an important role. It is therefore interesting to see what happens when the initial position of K is slightly shifted. This could occur either due to thermal excitation or to quantum delocalization. One can use diabatic potentials and ground state K wave function (see fig. 2.3) to determine the order of magnitude of a reasonable shift. It appears that both thermal (0.4 K) and quantum (half of the maximum of the wave function) fluctuations give a possible ± 0.5 Å shift for the excitation position.

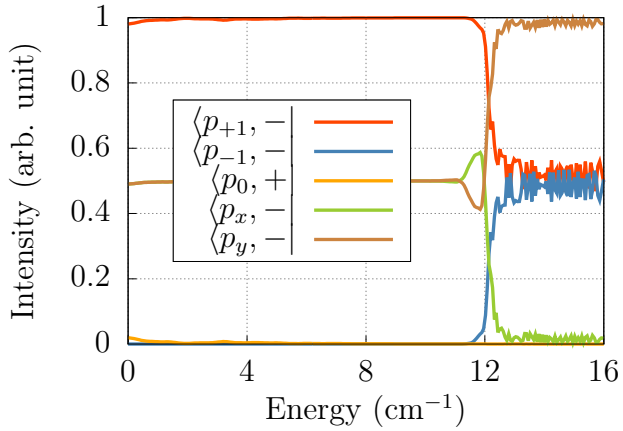

Figure 2.13 – Evolution of the electronic state as a function of time

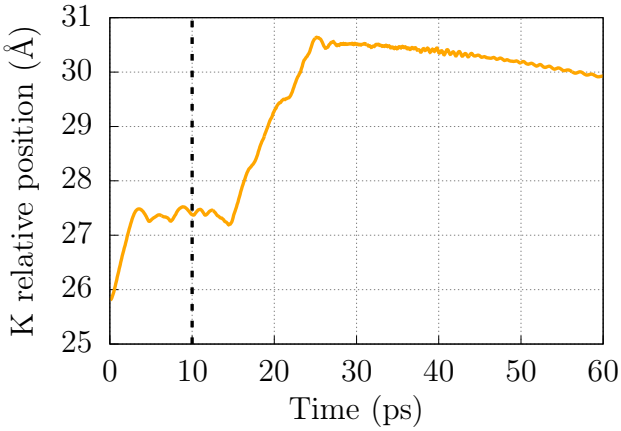

Figure 2.14 – Distance between K and He_N centers of mass as a function of time

When the initial position of the potassium atom is shifted by $+0.5$ Å, the dynamics is not affected. On the opposite, when it is shifted by -0.5 Å the situation is quite different. At first, we observe a linear exciplex formation in 5 ps (fig. 2.15a): helium atoms are attracted to K, and the internal state becomes a true eigenvector of L_z. It it worth noting that this exciplex shape can be explained: indeed the $|p_1\rangle$ orbital has an apple shape with a tiny well at the helium position. One may refer to [23] to get more details about orbital shapes and their link to exciplex formation.

The linear exciplex lasts for 10 ps. After that we can clearly see a symmetry breaking: the system is violently projected into an asymmetric $|p_y\rangle$ state (fig. 2.13), and we see formation of a ring exciplexe around this orbital (fig. 2.15b). This is clearly not expected, because our framework is of cylindrical symmetry and there is no physical reason to break it. It can be noted that this symmetry breaking happens along a well defined axis of our system. During the ring exciplex formation, we see unexplained high helium density between the droplet and the impurity in the ring plane that forces the exciplex to shift outward. This structure seems to disappear at long time and the exciplex is brought back closer (fig. 2.14). Our hypothesis is that this arises because we use a cubic grid with a step size of 0.4 Å which is not small enough to describe a 1 Å^3 exciplex in cylindrical symmetry. Unfortunately decreasing the the spatial step size quickly becomes too expensive in computing time and we cannot use a cylindrical grid (see the annex for detail).

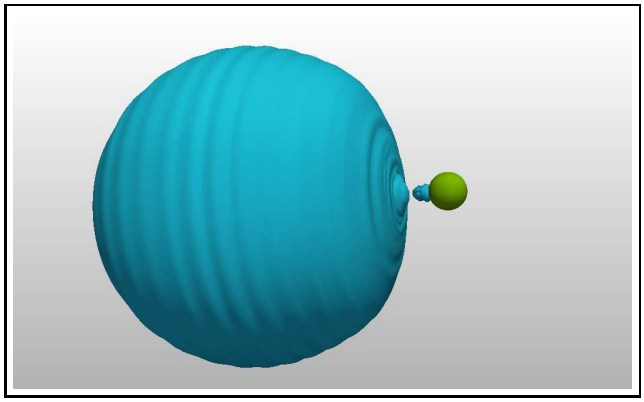

(a) Linear exciplex at $t = 7.5$ ps

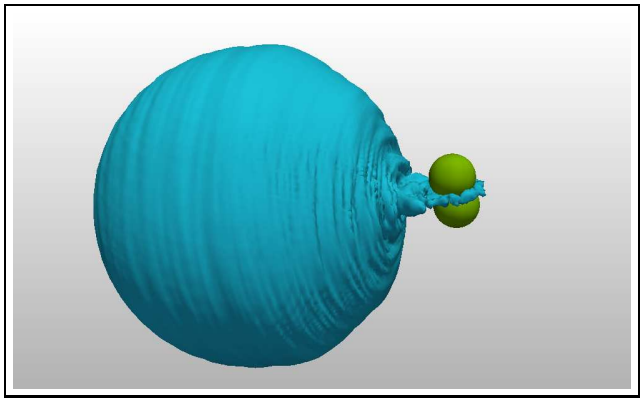

(b) Ring exciplex at $t = 19.5$ ps

Figure 2.15 – Snapshot of He_N density and bound K exciplex before and after the symmetry breaking, K p_y orbital is schematically represented in the second case to help the interpretation

Investigations on symmetry breaking

In order to test the hypothesis of the grid effect we worked with a smaller system (90 atoms) an studied the effect of grid size. As can be seen in table 2.1, the symmetry breaking occurs later and later as we reduce the mesh step size, which corroborates our hypothesis.

Spatial step size δr (Å)	0.42	0.28	0.21	0.14
Appearance of the symmetry breaking (ps)	3.2	5.6	9.0	10.8

Table 2.1 – Evolution of time before the occurrence of symmetry breaking during a dynamic simulation of $\Pi_{1/2}$ excitation for different spatial step sizes.

Now we can understand what is happening: the exciplex formation creates a high density volume which is poorly described by our cubic mesh. This induces asymmetry in the density profile at the surface of the droplet near to K, which induces back an asymmetric interaction and ends up in the projection of the internal state into an energetically more favorable configuration. This also explains why this projection occurs along a well defined axis of our simulation.

2.2.4 $\Pi_{3/2}$ exciplex formation: beyond symmetry breaking investigations

Exciplex formation and symmetry breaking

Exciting the $\Pi_{3/2}$ state leads without surprise to a linear exciplex (almost identical to fig. 2.15a) in 4 ps, because we excite in a potential well (fig. 1.4). However, in the exact same way as in the $\Pi_{1/2}$ we see that a symmetry breaking occurs. Looking at internal state projections (fig. 2.16) we see that before this symmetry breaking the internal state is actually pure in our basis, as it should, since the $\Omega = 3/2$ state is $|\lambda\rangle = |p_1, +\rangle$ (no other orbital can give $\Omega = 3/2$).

Comparing trajectories in the $\Pi_{1/2}$ (fig. 2.14) and in the $\Pi_{3/2}$ (fig. 2.17) states shows a difference: in the $\Pi_{3/2}$ state symmetry breaking occurs during an attempt to leave the droplet while in the $\Pi_{1/2}$ state it happens in a stationary position.

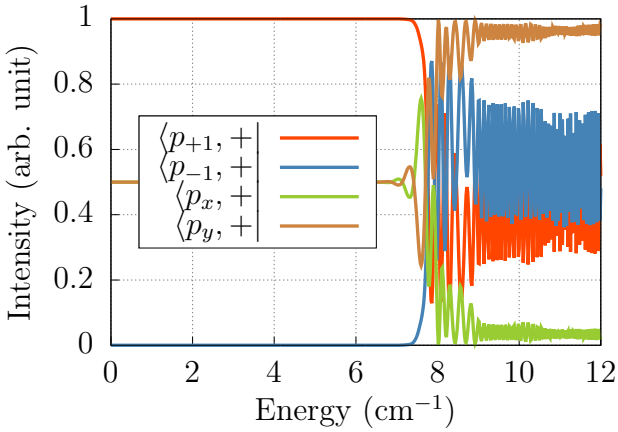

Figure 2.16 – Evolution of the electronic state as a function of time

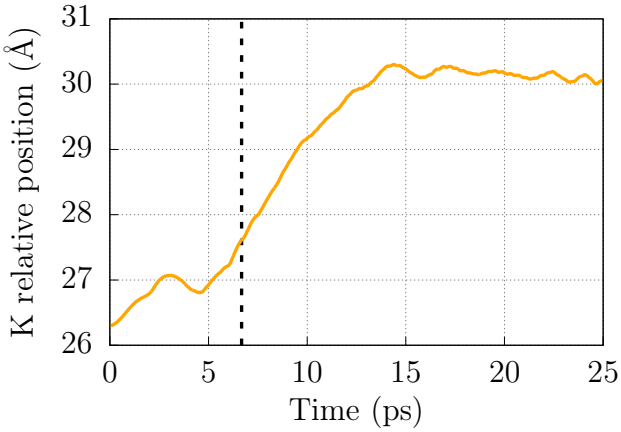

Figure 2.17 – Distance between K and He_N centers of mass as a function of time

Fixing internal state evolution

We can use the fact that there is no possible evolution for the internal state[2] to fix it instead of let it freely evolve. As can be seen in fig. 2.18, in that case the linear exciplex leaves the droplet after the symmetry breaking (fig. 2.18).

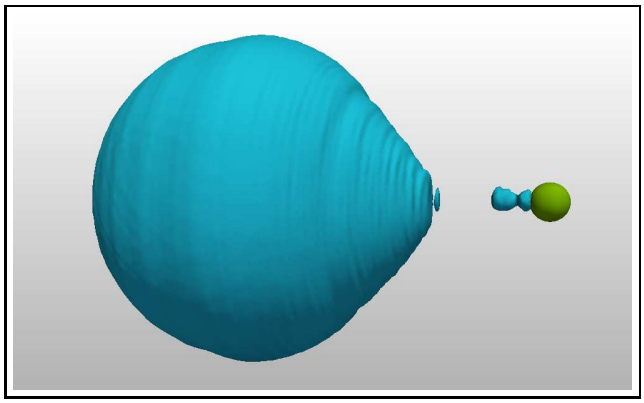

Figure 2.18 – Snapshot of He_N density with a linear KHe_n exciplex leaving the droplet at $t = 18.5$ ps

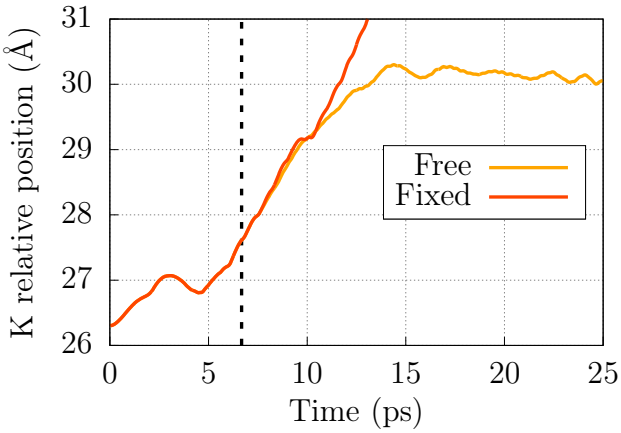

Figure 2.19 – Distance between K and He_N centers of mass as a function of time, for fixed and free $|\lambda\rangle$

Comparing trajectories in the case of a free or fixed electronic state evolution (fig. 2.19) shows that the leaving exciplex seems to be the natural response of this system. Nevertheless when we let the internal state evolve, the system finds a way to handle a new symmetry which is the formation of a ring exciplex that is more cubic symmetry friendly.

We might be tempted to interpret these symmetry breakings as a possibility that could occur in a real experiment, due to spatial distortion of the droplet or any external perturbation. Hints for ring exciplex stability in the Cs case have been found [23]. But this clearly remains an open question for potassium that requires further investigations.

[2] At least in our cylindrical framework

2.2.5 Comparison with exprimental data

Alkali doped droplets have been studied extensively [12–18, 22]. Nevertheless there are only two articles that investigated the dynamics following $4p \leftarrow 4s$ excitation of a K-doped droplet: [19, 20] (single article split in two) and [21]. [19, 20] collected dispersed emission spectra using reversed time-correlated single photon counting while [21] used femtosecond pumb-probe spectroscopy. Both report the formation of exciplexes in the Π states and desorption in the Σ state. Both show that the most abundant product species is KHe. They also report a $\sim$10% KHe_2 production. [21] even shows that KHe_n exciplexes are formed with $n = 3, 4$ (2.3% both) and $n = 5$ (0.5%). Nevertheless there is a huge discrepancy in the measured formation time scale. [19, 20] gives 50 ± 20 ps ($\Pi_{3/2}$) and 7.9 ns ($\Pi_{1/2}$), whereas [21] cannot resolve the two Π states but gives 180 ± 60 fs (KHe) and 204 ± 60 fs (KHe_2).

After discussions with the authors of [21] during a conference[3], it appears that their results on the time scale could be wrong due to a too high repetition rate of the exciting laser. They could have been exciting the $5p$ state (24701.382 cm^{-1} and 24720.139 cm^{-1} [27]) trough a two-photon process.

We have seen that our simulation describes well the formation of exciplexes. In particular the linear exciplex shape is consistent with the K-He observed experimentally[4] but no evidence for linear He-K-He (KHe_2) was found. The small proportion of higher n exciplexes observed experimentally could be a hint for the existence of ring shaped configurations.

Concerning the time scale in our simulations, in $\Pi_{3/2}$ excitation the potassium trajectory shows that the exciplex starts to leave within 5 ps, the symmetry breaking occurs after the beginning of desorption. Fixing the electronic state demonstrates that this desorption is the physical answer of the system rather than bound configuration. In the $\Pi_{1/2}$ state we observe a bouncing free potassium (the simulation is still running but the time scale to reach a stationary state may be $\sim$ ns). We could imagine that once in an equilibrium position, some tunneling effect may occur through the tiny barrier leading to exciplex formation within a few ns, see model presented in [19, 20]. Finally, in the displaced $\Pi_{1/2}$ we cannot fix the internal state but during the formation of the linear exciplex the internal state goes to $|p_1\rangle$, which is the same than in $\Pi_{3/2}$. This is why we can expect a departing exciplex (and not bound) within 15 ps.

These results are closer to the ones from [19, 20] which give 50 ps ($\Pi_{3/2}$) and 7.9 ns ($\Pi_{1/2}$) than [21] which give 180 fs for both. This is probably explained by the setup dysfunctional described earlier. The only true discrepancy that remains with [19, 20] is the $\Pi_{1/2}$ displaced excitation. We do not get a clear explanation, however as it is a turning point this could be a rare case in experiments. This could also be a limitation of our simulations.

2.3 Excitation towards $5s$ state

The last part of this study, which is still in progress, is the simulation of the $5s \leftarrow 4s$ photo-excitation. Since the ($5s$) state is isotropic, we could address this problem with both a classical and a quantum description for potassium.

[3] Quantum Fluid Clusters conference, Obergurgl (Austria), June 7-9, 2017, where I presented a poster on my results

[4] He-TDDFT has been found to give non-integer numbers of atom in exciplexes, so we may only use qualitative arguments based on 3D representation

2.3.1 Qualitative behavior and time scale

The first element that can be compared between the two approaches is the behavior of the potassium. In both cases it is ejected after excitation within 200 fs (fig. 2.20). This was actually highly predictable looking at the pair potential (fig. 1.3): it shows a potential energy of 700 K over the dissociation level (and in an isotropic state all helium-potassium pairs interact with the same potential). Nevertheless, we see that the asymptotic K velocity is not the same in quantum and classical description (fig. 2.21). We will investigate this point in the following paragraph.

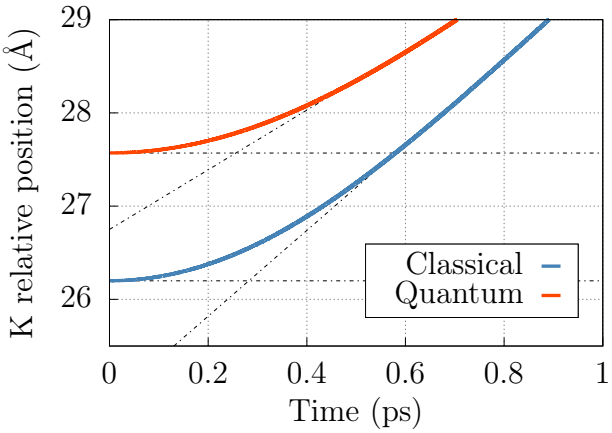

Figure 2.20 – Distance between classical/quantum K and He_N centers of mass as a function of time

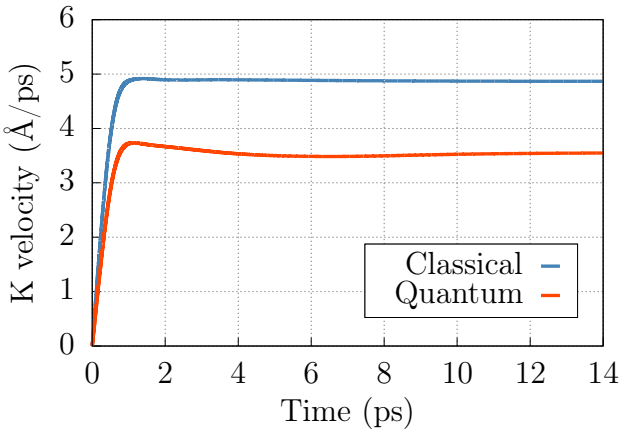

Figure 2.21 – Velocity of classical/quantum K and He_N as a function of time

2.3.2 Strongly interacting neighbor helium atoms

Let us consider a simple, impulsive model, which has already been used in the past [16]. K interacts with M neighboring He atoms. We assume that all the excitation energy ΔE (*id est* excess energy with respect to the dissociation threshold) is converted into kinetic energy. We can write both energy and momentum conservation

$$\frac{\mathbf{p}_{\mathrm{K}}^2}{2m\mathrm{K}} + \sum_{\mathrm{He}}^{M} \cdot \frac{\mathbf{p}_{\mathrm{He}}^2}{2m_{\mathrm{He}}} = \Delta E \tag{2.4}$$

$$\mathbf{p}_{\mathrm{K}} + \sum_{\mathrm{He}}^{M} \cdot \mathbf{p}_{\mathrm{He}} = 0 \tag{2.5}$$

Then we make the following assumption: all He momentum are equal, this is quite a huge approximation but this model is simple. Then some basic algebra gives an expression for M

$$\frac{\mathbf{p}_{\mathrm{K}}^2}{2m\mathrm{K}} = \frac{M \cdot m_{\mathrm{He}}}{m_K + M \cdot m_{\mathrm{He}}} \Delta E \equiv \alpha\, \Delta E \tag{2.6}$$

$$M = \frac{\alpha}{1-\alpha} \frac{m_{\mathrm{K}}}{m_{\mathrm{He}}} \tag{2.7}$$

In order to probe different excitation energies we have to shift the initial position of the potassium at excitation time. In the classical description of K we could study both diabatic or adiabatic helium density (*with frozen or relaxed helium density for the new position)*, while the quantum case will only be discussed within the adiabatic approximation, but the diabatic one is being studied currently.

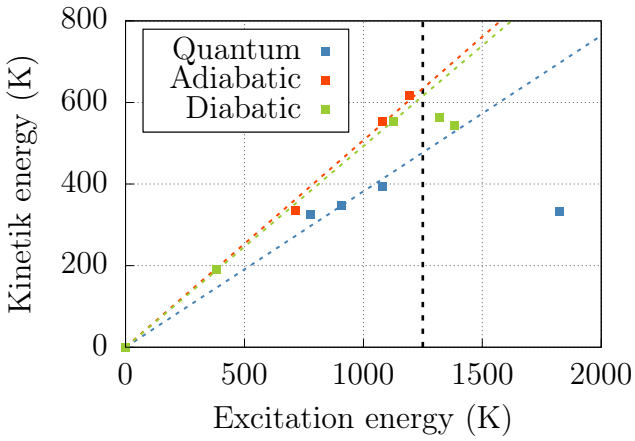

K motion	Quantum	Classical	
He density	Adiabatic	Adiabatic	Diabatic
α	0.38	0.50	0.49
M	6.03	10.06	9.49

Figure 2.22 – Asymptotic kinetic energy as a function of excitation energy, comparison between diabatic/adiabatic classical and quantum description, and table of values for linear fit

Our model seems to work well up to 1250 K then we see some non linear effects. It is presumably due to a large amount of energy exchange with the droplet, which can no longer be described as impulsive, hard-sphere like dissociation. We note that the classical description of K gives a higher number of neighboring helium atoms than the quantum one. This can be surprising at first, but if we look at the ground state density profile (fig. 2.1), we note that the edge is smoother, so the density of neighboring atoms is lower. Nevertheless we are still investigating this point. Finally, adiabatic and diabatic descriptions seem to give similar results in classical case. This means that changes in density imposed by K fluctuation in equilibrium state has more or less no consequence on final kinetic energy, which is not really surprising as we are looking for asymptotic value.

Conclusion

The first goal of this study was to investigate the $4p \leftarrow 4s$ photo-excitation of a potassium doping a droplet in order to compare with experiments. We have shown that the qualitative behavior reported in both references [19–21] was well described by our simulations. In particularly, the formation of exciplexes was observed in Π states and the ejection of a bare potassium atom in the Σ state. We noted that the spatial resolution and the cubic grid were not optimal to describe the cylindrical symmetry underlying exciplexes formation. This is why we only could make weak conclusions regarding the time scale, size and shape of exciplexes. Nevertheless, our results concerning their formation rate are clearly more consistent with [19, 20]. This conclusion has been corroborated in a direct exchange with the authors of [21]. They told us that they could have failed in properly time-resolving the excitation dynamics because of the high repetition rate of their laser at the time. Finally, both references observed a dominant production of K^*He exciplexes and a significant proportion (10 %) of K^*He_2 (and even larger exciplexes for [21]), while our simulations tend to show only K-He exciplex (before symmetry breaking). The physical relevance of ring exciplex formation after symmetry breaking is not clear and need to be clarified.

The second point that is still under investigation at the moment, is the $5s \leftarrow 4s$ photo-excitation. There is no experimental literature on this transition, this study is then purely predictive. We have performed two different simulations, one with the potassium atom treated as a classical and one as a quantum particle. We observed that the potassium behavior is the same in both descriptions: it is ejected quickly from the droplet within 0.2 ps. Nevertheless the asymptotic velocity is not the same. This is why we focused our comparison on the study of an impulsive model giving an estimate of the number of closest atoms directly interacting with the potassium at the time of photoexcitation. We have shown that the quantum case gave a lower number than the classical one, which explains that there is less momentum given to K.

To conclude, this work demonstrates once again that He-TDDFT coupled with DIM model is a very powerful tool to address the dynamics of helium droplets doped by an alkali atom upon photo-excitation. We could give a theoretical contribution to choose between the two contradictory experimental results. However, we also underlined difficulty of the 4HeDFT-BCN-TLS code in describing exciplex formation due to a simulation grid unadapted to the cylindrical symmetry at small scale. Finally, we started to describe the potassium desorption upon excitation to the $5s$ state. We hope that our results will motivate experimentalists to work on both transitions.

In a close future, we would like to study the $4p \leftarrow 4s$ transition with test particles in order to evaluate the importance of quantum effects in this case. We also want to address the question of the formation of a ring exciplex, and to finish our study of the $5s \leftarrow 4s$ transition. A long term motivation could be to rewrite part of the code to bypass the cubic limitation and get better results.

Annex: technical details on coding

The code we used is the 4He-DFT BCN-TLS [32]. A detailed description is provided in [31]. We give here the most important features about the computational approach. Equations are solved on a real space cubic grid. In order to compute the convolution products involved in the functional, we also work in FOURIER's space, which is why we use a cubic mesh.

a Imaginary time propagation

In order to find ground state properties we have to minimize a SCHRÖDINGER-like equation. Let us consider that we know the eigenvectors $\{\phi_k\}$ of the given Hamiltonian with energies $\{\varepsilon_k\}$

$$H\phi_k = \varepsilon_k \phi_k \tag{.8}$$

Since H does not depend on time, one can formally write the propagation in time of a given ψ as

$$i\hbar \frac{\partial}{\partial t}\psi = H\psi \Rightarrow \psi(t) = \mathrm{e}^{-i\frac{t}{\hbar}H}\,\psi(0) \tag{.9}$$

Let us now introduce an *imaginary time* as $\tau = it/\hbar$ and rewrite (eq. .9) as a function of τ

$$i\hbar \frac{\partial}{\partial \tau}\frac{\mathrm{d}\tau}{\mathrm{d}t}\psi = H\psi \Rightarrow \frac{\partial}{\partial \tau}\psi = -H\psi \Rightarrow \psi(\tau) = \mathrm{e}^{-\tau H}\,\psi(0) \tag{.10}$$

We expand $\psi(0)$ in the basis H eigenvectors

$$\psi(0) = \sum_{k=0}^{k=\infty} \alpha_k \phi_k \quad \text{and} \quad H\phi_k = \varepsilon_k\phi_k \Rightarrow \psi(\tau) = \sum_{k=0}^{k=\infty} \alpha_k\, \mathrm{e}^{-\tau\varepsilon_k}\,\phi_k \tag{.11}$$

What we see in eq. .11, is that upon propagation with imaginary time, only the ground state survives. In practice to compute $\psi(\tau)$ we use

$$\psi(\tau + \delta\tau) \approx (1 - \delta\tau H)\,\psi(\tau) \equiv \psi(\tau) + \delta\psi(\tau) \tag{.12}$$

This expression is iterated until convergence, which gives the ground state eigenvector and its associated eigenvalue

$$\varepsilon_0 = \frac{\langle\Psi|\,H\,|\Psi\rangle}{\langle\Psi|\Psi\rangle} \tag{.13}$$

b Real time propagation

To solve time dependent equations we use HAMMING's predictor-modifier-corrector method which is detailed in [33]. Let us consider a system of N ordinary differential equations

$$\dot{\mathbf{y}} \equiv \frac{\mathrm{d}\mathbf{y}}{\mathrm{d}x} = \mathbf{f}(x, \mathbf{y}) \quad \text{with} \quad \mathbf{f} : \mathbb{R}^{N+1} \to \mathbb{R}^N \quad \text{and} \quad \mathbf{y} \in \mathbb{R}^N \tag{.14}$$

We set $\mathbf{y}(x_0) = \mathbf{y}_0$ and we denote by h the x step. Higher order differential equations can be reduced to a system of coupled differential equations. We apply the following scheme whose error is $\mathcal{O}(h^5)$

$$\text{[Predictor]} \quad \mathbf{p}_{n+1} = \mathbf{y}_{n-3} + \frac{4h}{3}(2\dot{\mathbf{y}}_n - \dot{\mathbf{y}}_{n-1} + 2\dot{\mathbf{y}}_{n-2}) \tag{.15}$$

$$\text{[Modifier]} \quad \mathbf{m}_{n+1} = \mathbf{p}_{n+1} - \frac{112}{121}(\mathbf{p}_n - \mathbf{c}_n) \quad \text{and} \quad \dot{\mathbf{m}}_{n+1} = \mathbf{f}(x_{n+1}, \mathbf{m}_{n+1}) \tag{.16}$$

$$\text{[Corrector]} \quad \mathbf{c}_{n+1} = \frac{1}{8}(9\mathbf{y}_n - \mathbf{y}_{n-2} + 3h(\dot{\mathbf{m}}_{n+1} + 2\dot{\mathbf{y}}_n - \dot{\mathbf{y}}_{n-1})) \tag{.17}$$

$$\text{[Final value]} \quad \mathbf{y}_{n+1} = \mathbf{c}_{n+1} + \frac{9}{121}(\mathbf{p}_{n+1} - \mathbf{c}_{n+1}) \tag{.18}$$

The main advantage of this algorithm is that it only requires two evaluations of $\mathbf{f}$ per step and this is the time consuming part of our calculation. Nevertheless note that is a not a self starting method, it requires values from three preceding steps (see eq. .15). We need to be at least as accurate than $\mathcal{O}(h^5)$ this is why we initialize the computation by using Runge-Kutta-Gill method

$$\mathbf{k}_1 = h\,\mathbf{f}(x_n, y_n) \tag{.19}$$

$$\mathbf{k}_2 = h\,\mathbf{f}\left(x_n + \frac{h}{2}, \mathbf{y}_n + \frac{1}{2}\,\mathbf{k}_1\right) \tag{.20}$$

$$\mathbf{k}_3 = h\,\mathbf{f}\left(x_n + \frac{h}{2}, \mathbf{y}_n + (-1+\sqrt{2}),\mathbf{k}_1 + \left(1 - \frac{\sqrt{2}}{2}\right)\mathbf{k}_2\right) \tag{.21}$$

$$\mathbf{k}_4 = h\,\mathbf{f}\left(x_n + h, \mathbf{y}_n - \frac{\sqrt{2}}{2}\,\mathbf{k}_2 + \left(1 + \frac{\sqrt{2}}{2}\right)\mathbf{k}_3\right) \tag{.22}$$

$$\mathbf{y}_{n+1} = \mathbf{y}_n + \frac{1}{6}\left(\mathbf{k}_1 + (2-\sqrt{2})\,\mathbf{k}_2 + (2+\sqrt{2})\,\mathbf{k}_3 + \mathbf{k}_4\right) + \mathcal{O}(h^5) \tag{.23}$$

We do not discuss here the boundary conditions, in particular how we can deal with helium leaving the droplet, because it is beyond the scope of this annex, this is explained in details in [31].

c Simulating spectra

The width of absorption spectrum is the result of helium density and potassium wave function fluctuations. In order to simulate this spectrum, we use the DF sampling method, the interested reader should refer to [34].

One can write, using the time dependent formulation, that within the Born-Oppenheimer approximation, the intensity associated with an electronic transition from a state i to a state f writes as

$$I(\omega) \propto \int \mathrm{d}t\, \mathrm{e}^{i(\omega+\omega_i)t} \int \mathrm{d}\mathbf{r}\, (\mu_{f\leftarrow i}\,\phi_i)^*\, \mathrm{e}^{-iH_f t/\hbar}\, (\mu_{f\leftarrow i}\,\phi_i) \tag{.24}$$

In this expression ϕ_i refers to the eigenfunction of potassium in the initial state with energy $\hbar\omega_i$, $\mu_{f\leftarrow i}$ is the electronic transition dipole and H_f is the potassium Hamiltonian in the final state that can written as a sum of kinetic and potential energy $H = T + V(\mathbf{r}_\mathrm{K})$.

We can then expand ϕ in a basis of eigenvectors $\alpha_\nu(\mathbf{r})$ H_f, which gives an expression for the intensity

$$\phi(\mathbf{r}) = \sum_\nu a_\nu \alpha_\nu(\mathbf{r}) \quad \text{with} \quad a_\nu = \int \mathrm{d}\mathbf{r}\, \alpha_\nu^*(\mathbf{r}) \phi_i(\mathbf{r}) \tag{.25}$$

$$I(\omega) = \sum_\nu |a_\nu|^2 \, \delta(\omega - (\omega_\nu - \omega_i)) \tag{.26}$$

This gives a spectrum of lines with energies $\hbar(\omega_\nu - \omega_i)$ and relative intensities $|a_\nu|^2$ which are the so-called FRANCK-CONDON factors . Considering that the final states are a quasi-continuous spectrum of H_f, it can be assumed that kinetic contribution is negligible. Then we can integrate over time and we obtain the semi-classical expression for the intensity, which is often called *reflection principle*.

$$I(\omega) = \int \mathrm{d}\mathbf{r}\, |\phi_i(\mathbf{r})|^2 \, \delta\left(\omega - \left(\frac{V(\mathbf{r})}{\hbar} - \omega_i\right)\right) \tag{.27}$$

In order to evaluate this expression, we randomly generate n_c configuration of N positions for the helium atoms and one for potassium. The helium positions are generated from the converged density with a hard-sphere repulsion (exclusion volume with radius 2.18 Å) which is supposed to represent the He-He correlation (one may actually refer to [31] because the radius of exclusion is chosen density-dependent, but this is beyond the scope of this simple explanation). The potassium position can be either generated from its wave function in a quantum treatment or from its classical position. For a given sampled configuration $\{k\}$ the transition energy is

$$E\{k\} = V_f\{k\} - V_i\{k\} \tag{.28}$$

where V corresponds to a sum over pair interactions which is written as $E_{ij\alpha\beta}^{nl}$ in eq. 1.22 with $\{nl, i, j, \alpha, \beta\}$ fixed by the state we are interested in. Finally we get the spectrum by collecting each configuration contribution in a histogram.

$$I(\omega) \propto \frac{1}{n_c} \sum_{\{k\}} \delta\left(\omega - \frac{E\{k\}}{\hbar}\right) \tag{.29}$$

d Values of functional parameters

Name	Units	Value
$\varepsilon_{\mathrm{LJ}}$	K	10.22
σ	Å	2.556
h	Å	2.190323
c_2	KÅ^6	-2.41186×10^4
c_3	KÅ^9	1.85850×10^6
α_s	Å^3	54.31
ρ_0	Å^{-3}	0.04
l	Å	1.0

C	Hartree	0.1
β	Å^3	40.0
ρ_m	Å^{-3}	0.37
γ_{11}		-19.7544
γ_{12}	Å^{-2}	15.5616
α_1	Å^{-2}	1.023
γ_{21}		-0.2395
γ_{22}	Å^{-2}	0.0312
α_2	Å^{-2}	0.14912

Table 1 – Parameters value of the different functional

Bibliography

[1] J. Peter Toennies, Andrej F. Vilesov and K. Birgitta Whaley. 'Superfluid Helium Droplets: An Ultracold Nanolaboratory'. In: *Physics Today* 54.2 (2001), pp. 31–37. DOI: 10.1063/1.1359707. eprint: http://dx.doi.org/10.1063/1.1359707. URL: http://dx.doi.org/10.1063/1.1359707.

[2] J. Peter Toennies and Andrey F. Vilesov. 'Superfluid Helium Droplets: A Uniquely Cold Nanomatrix for Molecules and Molecular Complexes'. In: *ChemInform* 35.27 (2004). un commentaire, no–no. ISSN: 1522-2667. DOI: 10.1002/chin.200427197. URL: http://dx.doi.org/10.1002/chin.200427197.

[3] Manuel Barranco et al. 'Helium Nanodroplets: An Overview'. In: *Journal of Low Temperature Physics* 142.1 (2006), p. 1. ISSN: 1573-7357. DOI: 10.1007/s10909-005-9267-0. URL: http://dx.doi.org/10.1007/s10909-005-9267-0.

[4] M. Hartmann et al. 'Rotationally Resolved Spectroscopy of SF_6 in Liquid Helium Clusters: A Molecular Probe of Cluster Temperature'. In: *Phys. Rev. Lett.* 75 (8 1995), pp. 1566–1569. DOI: 10.1103/PhysRevLett.75.1566. URL: https://link.aps.org/doi/10.1103/PhysRevLett.75.1566.

[5] S. Grebenev et al. 'Spectroscopy of molecules in helium droplets'. In: *Physica B: Condensed Matter* 280.1 (2000), pp. 65 –72. ISSN: 0921-4526. DOI: http://dx.doi.org/10.1016/S0921-4526(99)01451-9. URL: http://www.sciencedirect.com/science/article/pii/S0921452699014519.

[6] Luis F. Gomez et al. 'Shapes and vorticities of superfluid helium nanodroplets'. In: *Science* 345.6199 (2014), pp. 906–909. ISSN: 0036-8075. DOI: 10.1126/science.1252395. eprint: http://science.sciencemag.org/content/345/6199/906.full.pdf. URL: http://science.sciencemag.org/content/345/6199/906.

[7] F. Ancilotto et al. In: *Int. Review in Phys. Chem.* (2017), to be published.

[8] Daniel J. Merthe and Vitaly V. Kresin. 'Electrostatic Deflection of a Molecular Beam of Massive Neutral Particles: Fully Field-Oriented Polar Molecules within Superfluid Nanodroplets'. In: *The Journal of Physical Chemistry Letters* 7.23 (2016). PMID: 27934050, pp. 4879–4883. DOI: 10.1021/acs.jpclett.6b02401. eprint: http://dx.doi.org/10.1021/acs.jpclett.6b02401. URL: http://dx.doi.org/10.1021/acs.jpclett.6b02401.

[9] Benjamin Shepperson et al. 'Strongly aligned molecules inside helium droplets in the near-adiabatic regime'. In: *The Journal of Chemical Physics* 147.1 (2017), p. 013946. DOI: 10.1063/1.4983703. eprint: http://dx.doi.org/10.1063/1.4983703. URL: http://dx.doi.org/10.1063/1.4983703.

[10] Alexander Volk et al. 'The impact of doping rates on the morphologies of silver and gold nanowires grown in helium nanodroplets'. In: *Phys. Chem. Chem. Phys.* 18 (3 2016), pp. 1451–1459. DOI: 10.1039/C5CP06248A. URL: http://dx.doi.org/10.1039/C5CP06248A.

[11] J. Higgins et al. 'Helium Cluster Isolation Spectroscopy of Alkali Dimers in the Triplet Manifold'. In: *The Journal of Physical Chemistry A* 102.26 (1998), pp. 4952–4965. DOI: 10.1021/jp981115g. eprint: http://dx.doi.org/10.1021/jp981115g. URL: http://dx.doi.org/10.1021/jp981115g.

[12] F. Stienkemeier et al. 'Spectroscopy of alkali atoms (Li, Na, K) attached to large helium clusters'. In: *Zeitschrift für Physik D Atoms, Molecules and Clusters* 38.3 (1996), pp. 253–263. ISSN: 1431-5866. DOI: 10.1007/s004600050090. URL: http://dx.doi.org/10.1007/s004600050090.

[13] F. Lackner et al. 'Spectroscopy of nS, nP, and nD Rydberg series of Cs atoms on helium nanodroplets'. In: *Phys. Chem. Chem. Phys.* 13 (42 2011), pp. 18781–18788. DOI: 10.1039/C1CP21280J. URL: http://dx.doi.org/10.1039/C1CP21280J.

[14] Florian Lackner et al. 'Rubidium on Helium Droplets: Analysis of an Exotic Rydberg Complex for $n^* < 20$ and $0 \leq l \leq 3$'. In: *The Journal of Physical Chemistry Letters* 3.10 (2012). PMID: 26286790, pp. 1404–1408. DOI: 10.1021/jz300381y. eprint: http://dx.doi.org/10.1021/jz300381y. URL: http://dx.doi.org/10.1021/jz300381y.

[15] F. R. Brühl, R. A. Trasca and W. E. Ernst. 'Rb–He exciplex formation on helium nanodroplets'. In: *The Journal of Chemical Physics* 115.22 (2001), pp. 10220–10224. DOI: 10.1063/1.1410118. eprint: http://aip.scitation.org/doi/pdf/10.1063/1.1410118. URL: http://aip.scitation.org/doi/abs/10.1063/1.1410118.

[16] Alberto Hernando et al. 'Desorption of alkali atoms from 4He nanodroplets'. In: *Phys. Chem. Chem. Phys.* 14 (11 2012), pp. 3996–4010. DOI: 10.1039/C2CP23526A. URL: http://dx.doi.org/10.1039/C2CP23526A.

[17] Evgeniy Loginov and Marcel Drabbels. 'Dynamics of Excited Sodium Atoms Attached to Helium Nanodroplets'. In: *The Journal of Physical Chemistry A* 118.15 (2014). PMID: 24673631, pp. 2738–2748. DOI: 10.1021/jp4121996. eprint: http://dx.doi.org/10.1021/jp4121996. URL: http://dx.doi.org/10.1021/jp4121996.

[18] Evgeniy Loginov et al. 'Excitation of Sodium Atoms Attached to Helium Nanodroplets: The 3p ← 3s Transition Revisited'. In: *The Journal of Physical Chemistry A* 119.23 (2015). PMID: 25582680, pp. 6033–6044. DOI: 10.1021/jp511885t. eprint: http://dx.doi.org/10.1021/jp511885t. URL: http://dx.doi.org/10.1021/jp511885t.

[19] J. Reho et al. 'Alkali–helium exciplex formation on the surface of helium nanodroplets. I. Dispersed emission spectroscopy'. In: *The Journal of Chemical Physics* 113.21 (2000), pp. 9686–9693. DOI: 10.1063/1.1321033. eprint: http://dx.doi.org/10.1063/1.1321033. URL: http://dx.doi.org/10.1063/1.1321033.

[20] J. Reho et al. 'Alkali–helium exciplex formation on the surface of helium nanodroplets. II. A time-resolved study'. In: *The Journal of Chemical Physics* 113.21 (2000), pp. 9694–9701. DOI: 10.1063/1.1321034. eprint: http://dx.doi.org/10.1063/1.1321034. URL: http://dx.doi.org/10.1063/1.1321034.

[21] C. P. Schulz, P. Claas and F. Stienkemeier. 'Formation of K^*He Exciplexes on the Surface of Helium Nanodroplets Studied in Real Time'. In: *Phys. Rev. Lett.* 87 (15 2001), p. 153401. DOI: 10.1103/PhysRevLett.87.153401. URL: http://link.aps.org/doi/10.1103/PhysRevLett.87.153401.

[22] Johannes von Vangerow et al. 'Imaging Excited-State Dynamics of Doped He Nanodroplets in Real-Time'. In: *The Journal of Physical Chemistry Letters* 8.1 (2017). PMID: 27996261, pp. 307–312. DOI: 10.1021/acs.jpclett.6b02598. eprint: http://dx.doi.org/10.1021/acs.jpclett.6b02598. URL: http://dx.doi.org/10.1021/acs.jpclett.6b02598.

[23] Mohamed Zbiri and Claude Daul. 'Theoretical investigation of the $Cs^*He_{n\geqslant 3}$ exciplexes'. In: *Physics Letters A* 341.1 (2005), pp. 170 –176. ISSN: 0375-9601. DOI: http://dx.doi.org/10.1016/j.physleta.2005.04.066. URL: http://www.sciencedirect.com/science/article/pii/S0375960105006286.

[24] P. Hohenberg and W. Kohn. 'Inhomogeneous Electron Gas'. In: *Phys. Rev.* 136 (3B 1964), B864–B871. DOI: 10.1103/PhysRev.136.B864. URL: https://link.aps.org/doi/10.1103/PhysRev.136.B864.

[25] F. Ancilotto et al. 'Freezing of ^{4}He and its liquid-solid interface from density functional theory'. In: *Phys. Rev. B* 72 (2005), p. 214522. DOI: 10.1103/PhysRevB.72.214522. URL: http://link.aps.org/doi/10.1103/PhysRevB.72.214522.

[26] Frank O. Ellison. 'A Method of Diatomics in Molecules. I. General Theory and Application to H2O'. In: *Journal of the American Chemical Society* 85.22 (1963), pp. 3540–3544. DOI: 10.1021/ja00905a002. eprint: http://dx.doi.org/10.1021/ja00905a002. URL: http://dx.doi.org/10.1021/ja00905a002.

[27] A. Kramida et al. NIST Atomic Spectra Database (ver. 5.3), [Online]. Available: http://physics.nist.gov/asd [2017, June 20]. National Institute of Standards and Technology, Gaithersburg, MD. 2015.

[28] J. Pascale. 'Use of l-dependent pseudopotentials in the study of alkali-metal-atom—He systems. The adiabatic molecular potentials'. In: *Phys. Rev. A* 28 (2 1983), pp. 632–644. DOI: 10.1103/PhysRevA.28.632. URL: https://link.aps.org/doi/10.1103/PhysRevA.28.632.

[29] S. H. Patil. 'Adiabatic potentials for alkali–inert gas systems in the ground state'. In: *The Journal of Chemical Physics* 94.12 (1991), pp. 8089–8095. DOI: 10.1063/1.460091. eprint: http://dx.doi.org/10.1063/1.460091. URL: http://dx.doi.org/10.1063/1.460091.

[30] Erich Runge and E. K. U. Gross. 'Density-Functional Theory for Time-Dependent Systems'. In: *Phys. Rev. Lett.* 52 (12 1984), pp. 997–1000. DOI: 10.1103/PhysRevLett.52.997. URL: https://link.aps.org/doi/10.1103/PhysRevLett.52.997.

[31] M. Barranco et al. *Zero temperature DFT and TDDFT for 4He: A short guide for practitioners*. URL: https://github.com/bcntls2016/DFT-Guide/blob/master/dft-guide.pdf.

[32] M. Pi et al. *4He-DFT BCN-TLS: A Computer Package for Simulating Structural Properties and Dynamics of Doped Liquid Helium-4 Systems*. 2016. URL: https://github.com/bcntls2016.

[33] A. Ralston and H. S. Wilf. *Mathematical methods for digital computers*. 1960.

[34] David Mateo et al. 'Absorption spectrum of atomic impurities in isotopic mixtures of liquid helium'. In: *Phys. Rev. B* 83 (17 2011), p. 174505. DOI: 10.1103/PhysRevB.83.174505. URL: https://link.aps.org/doi/10.1103/PhysRevB.83.174505.